Chapter 11

Sample Resonators for Quasioptical EPR

A Practical Guide for Biological Applications

David E. Budil[1] and Keith A. Earle[2]

[1]*Dept. of Chemistry and Chemical Biology, Northeastern University, Boston MA 02115,*
[2]*Dept. of Chemistry and Chemical Biology, Cornell University, Ithaca NY 14853*

Abstract: A review of sample holders and sample cavities for application of quasioptical high field, high frequency electron paramagnetic resonance to biological samples.

Key words: cavity, quasioptical, high field EPR, high frequency EPR, Fabry-Pérot, sensitivity

1. INTRODUCTION AND OVERVIEW

There has been a remarkable growth of high-field, high frequency (HF) EPR methods over the past decade (for recent reviews see (Earle *et al.*, 1996a; Doubinski 1998; Earle and Freed 1999; Eaton and Eaton 1999; Smith and Riedi 2000)). Spectrometers based on standard waveguide-based designs operating at frequencies up to 150 GHz are now commercially available. At higher frequencies, the spectrometer designs that are currently in use have been more diverse, although they seem to be converging to a standard bridge design based on quasioptical methods that is also commercially available.

However, a much wider variety of cavity and sample arrangements are currently employed in EPR spectrometers at the highest fields, and a number of new and interesting devices are still under active development. The broad range of options and opportunities available motivates the need to survey the different sample cavities that may be used in quasioptical EPR for investigators in the field.

The choice of sample arrangement for quasioptical EPR depends strongly upon the application for which it is intended, as well as the design of the EPR

FROM:
Biological Magnetic Resonance, Vol. 22, Very High Frequency (VHF) ESR/EPR
Edited by: Oleg Grinberg and Lawrence J. Berliner
Kluwer Academic/Plenum Pub. 2004

bridge. The most important considerations in selecting a design include one or more of the following: (1) signal sensitivity, either concentration or absolute sensitivity, (2) sensitivity to grain size in powder samples, (3) millimetre-wave field strength at the sample, (4) isolation between cavity and detector or oscillator, (5) compatibility with overall spectrometer design, including reflection, transmission, and broadband designs, (6) provision for magnetic field modulation, rf irradiation for ENDOR, sample illumination, sample alignment, sample rotation, or application of electric fields, and (7) ease of sample handling and fabrication. Any given cavity design may be optimal for only a selected few of these criteria; thus, it is worthwhile to prioritize the desired performance characteristics for a given application before selecting which type of cavity is to be used.

This chapter is an effort to survey the growing variety of options that are currently available for accommodating samples in quasioptical high-field EPR applications. After a review of the general contributions of cavities to sensitivity in the context of high-frequency EPR, we survey the cavity configurations that have been most frequently and successfully applied to biological systems. The particular strengths and weaknesses of each design will be briefly presented and compared, and where possible, quantitative information will be given to assist the reader with specific designs for new sample types and EPR frequencies. The chapter concludes with the presentation of a method for designing cavities for aqueous samples, a problem of considerable importance for high-field EPR of biological samples.

2. CAVITY CONTRIBUTIONS TO SENSITIVITY

2.1 Absolute Sensitivity

Of the various criteria used to evaluate cavity performance, the most important is sensitivity. Here, only the cavity contributions to overall spectrometer sensitivity will be considered. The most common measure of high-field spectrometer performance is the absolute sensitivity, which is defined as the minimum number of spins N_{min} that give a signal-to-noise ratio of 1 for a line with a 1 G line width and a 1 Hz detection bandwidth. Neglecting saturation effects, N_{min} is given by the expression (Poole 1983; Earle *et al.*, 1996a)

$$N_{\min} = \frac{2V_s k_B T_S (2I+1)}{g^2 \beta_e^2 S(S+1)} \left(\frac{\Delta\omega}{\omega}\right) \left(\frac{\Delta H_{pp}}{H_{\mathrm{mod}}}\right) \left(\frac{1}{\eta Q_L}\right) \left(\frac{1}{M}\right) \left(\frac{k_B T_D \Delta f}{P_0}\right)^{1/2} \quad [1]$$

where V_S is the sample volume, k_B is Boltzmann's constant, T_S is the sample temperature, g is the electronic g-factor, S is the total electron spin, I is the nuclear spin, β is the Bohr magneton, ω is the electronic Larmor frequency, $\Delta\omega$ is the linewidth, ΔH_{mod} is the Zeeman field modulation amplitude, ΔH_{pp} is the derivative peak-to-peak linewidth, η is the filling factor (defined below), Q_L is the loaded cavity Q, T_D is the effective detector noise temperature, Δf is the detector input bandwidth, P_0 is the incident mm-wave power, and M is a matching factor that depends upon the type of cavity (reflection, transmission, or induction, as discussed in further detail below):

$$M_{trans} = \frac{\sqrt{\beta_1\beta_2}}{(1+\beta_1+\beta_2)}$$
$$M_{refl} = \frac{\beta}{(1+\beta)} \qquad [2]$$
$$M_{ind} = \frac{\sqrt{\beta_1\beta_2}}{(1+\beta_1)(1+\beta_2)}$$

where β_1 and β_2 are cavity input and output coupling factors, and $\beta_1 \equiv \beta$, $\beta_2 = 0$ for a reflection cavity). In the case of the induction mode cavity, "input" and "output" may refer to different polarization states at a single coupling element such as an iris or coupling mirror, and are equal for cylindrically symmetrical elements.

To facilitate comparison of the effects of cavity properties and geometry on sensitivity, the filling factor η into two contributions following Poole 1983:

$$\eta \equiv \frac{\int_{V_s} H_1^2 dV}{\int_{V_c} H_1^2 dV} = \frac{V_s\langle H_S^2\rangle}{V_C\langle H_C^2\rangle} \equiv \frac{V_S}{V_C} R_H \qquad [3]$$

where V_C is the cavity volume and the field intensity factor $R_H \equiv \langle H_S^2\rangle/\langle H_C^2\rangle$ is the ratio of the average squared value of the "useful" H field (i.e. the component orthogonal to the spectrometer field) over the sample compared to the average squared H-field in the cavity.

Poole 1983, has calculated the R_H parameter for the two single-mode cavities that are most commonly used in waveguide-based EPR, namely a cylindrical TE_{011} and a rectangular TE_{102} cavity, containing point, cylindrical, and cavity-filling samples. In order to compare these cases with quasioptical cavities, the "flat" sample type has been added, and calculations of R_H for the Fabry-Pérot

and non-resonant sample holders carried out for all of these of the sample types. The results are shown in *Table 1.*

Typical dimensions were used for each of the cavities shown in *Table 1*, and scaled according to wavelength as follows. The TE_{011} cylindrical cavity was taken to have radius a and length $d=2a$, so that $\lambda = 1.52\ a$ at resonance, and $V_C = 1.88\lambda^3$. For the TE_{102} rectangular cavity with cross-sectional dimensions a and $b=a/2$ and length $d=2a$, $\lambda = \sqrt{2}a$ at resonance, giving $V_C = 0.354\lambda^3$. The TEM_{006} Fabry-Pérot resonator was assumed to have a beam waist $w = 2\lambda$ at the sample, which was also taken as the effective radius to define the cavity volume, $V_C = 37.7\lambda^3$ Finally, the non-resonant holder was taken to have a cylindrical shape with radius equal to 2λ and length of 6λ, giving the same effective volume as the Fabry-*Pérot* cavity.

Table 1. Field Intensity Factor R_H and Volume Ratio V_S/V_C for Selected Typical Cavity and Sample Configurations

Cavity type	Sample Type[a]				
	Point	Cylindrical		Flat	
		R_H	V_S/V_C	R_H	V_S/V_C
Cylindrical TE_{011}	10.6	5.1	0.0050	1.0	0.015
Rectangular TE_{102}	2.00	1.0	0.028	1.0	0.089
Fabry-Pérot TEM_{006}	2.4	1.3	0.00074	1.0	0.0067
Non-resonant	2.4	1.3	0.00074	1.0	0.0067

(a) For cylindrical and flat sample types, upper number is field intensity factor R_H and lower number is volume ratio V_S/V_C

Recent work at Cornell University on Fabry-*Pérot* resonators has focused on reducing the effective resonator volume in order to maximize the achievable B_1 at the sample. In one system that is currently under test, the beam waist $w = \lambda$ at the sample. The longitudinal mode number $q = 4$. Under those conditions, the effective resonator volume is $V_C \approx \pi\lambda^3$, which should be compared with the standard cavity designs discussed above. Initial results from simple pulse experiments at 95GHz using this developmental resonator have shown great promise, but more work needs to be done to characterize fully the performance of this novel design. Our point in mentioning this provisional resonator design is to indicate ways in which Fabry-*Pérot* resonators can compete with standard cavity designs. We will not discuss it further here.

The sample geometries were also scaled according to wavelength, as follows: (1) *point samples* were situated at the point of highest B_1 (2) *cylindrical samples* (e.g. a sample in a capillary tube) were taken to have radius $r = \lambda/15$, and situated along the axis of cylindrical cavities, at the beam waist but

transverse to the beam direction in Fabry-Pérot resonators and non-resonant holders, and along the *a* dimension through the centre of rectangular cavities; (3) *thin layer samples* were taken to have thickness $\lambda/50$, situated perpendicular to the *z* axis (*d* dimension) of cylindrical or rectangular cavities and perpendicular to the beam propagation direction in Fabry-Pérot and non-resonant systems; and (4) *cavity-filling samples* were assumed to fill the volume of each cavity type as defined above.

To compare the absolute sensitivity of different cavities using the information in *Table 1*, we collect all of the contributions in Eq. [1] that do not depend explicitly upon cavity parameters (i.e., detector and sample characteristics, input power, H_{mod} / ΔH_{pp}, etc.) into a constant κ so that we may write

$$N_{min} = \kappa\lambda\left(\frac{V_C}{R_H Q_L}\right)\left(\frac{1}{M}\right) \qquad [4]$$

Since higher sensitivity corresponds to smaller N_{min}, a figure of merit (FOM) F_A may be defined for comparing the absolute sensitivities of different cavities under equivalent conditions

$$F_A = MR_H Q_L \frac{1}{V_C}\frac{1}{\lambda} \qquad [5]$$

With this definition, $N_{min} = K/F_A$, and a higher FOM corresponds to a lower N_{min} and greater sensitivity. This FOM is tabulated for each cavity type described below in *Table 2*, together with the FOM for concentration sensitivity and B_1 field, described in the next two sections.

Absolute sensitivity is most important for samples that are only available in small amounts, such as single crystals, or samples for which the volume is limited by availability, high dielectric losses, or electrical conductivity. Many samples of biological importance fall into this category. The limiting factor in these cases (neglecting saturation effects) is the magnitude of the rf field at the sample, and the sensitivity becomes proportional to B_{rf}.

2.2 Concentration Sensitivity

Concentration sensitivity is defined as the minimum number of spins per unit volume that give a signal-to-noise ratio of 1 for a line with a 1 G line width and a 1 Hz detection bandwidth. Rewriting Eq. [4] to represent this quantity gives

$$\frac{N_{min}}{V_S} = K\lambda\left(\frac{V_C}{V_S R_H Q_L}\right)\left(\frac{1}{M}\right) \quad [6]$$

this leads to a somewhat different FOM for concentration sensitivity,

$$F_C = MR_H Q_L \frac{V_S}{V_C}\frac{1}{\lambda} \quad [7]$$

This figure is also tabulated for each cavity type below. Eq. [7] shows that the sample volume V_S plays an important role in determining the cavity concentration sensitivity. Concentration sensitivity is therefore the most appropriate figure of merit for samples where the volume is not restricted, such as powder samples. It is also important when the sample permits a high cavity Q, as is generally the case for low dielectric loss solids and liquids. There are two major sample types of biological interest for which it is most desirable to optimize concentration sensitivity, as outlined in the following two subsections.

2.2.1 Low Loss Samples

For low dielectric loss samples, the best strategy is to boost the concentration sensitivity by filling the sample-holders to the maximum practicable extent, thus maximizing V_S/V_C in Eq. [7]. In this case, single-mode and overmoded resonators are often the most effective solutions, and even non-resonant sample holders can become competitive under the right conditions.

2.2.2 Aqueous Samples

A broad selection of biologically important samples fall into a category where the sample has low spin concentration and high dielectric loss (e.g., aqueous samples) but is not severely limited in terms of its volume. In this case, optimal concentration sensitivity is most desirable, but there are additional constraints on the size of the sample that are imposed by its loss characteristics. For such cases, the Fabry-Pérot resonator is typically much more competitive than single-mode resonators. This can be understood by the following qualitative argument. Suppose that the characteristic distance by which the E-field may penetrate the sample at a given frequency is δ. In order to avoid the E-field lines in a cylindrical TE_{011} cavity mode, the sample must occupy a region within a distance δ of the cavity axis, with cross-sectional area $\pi\delta^2$. In the Fabry-Pérot, the sample must occupy a region within a distance δ of a node in the E-field standing wave, with thickness 2δ. Thus, the factor V_s/V_c in Eq. [7] is proportional to δ/λ for the Fabry-Pérot, but proportional to δ^2/λ^2 for the

cylindrical resonator. The higher the losses in the sample are, the smaller δ becomes, and the bigger is the advantage of the Fabry-Pérot for lossy samples. A procedure for optimizing Fabry-Pérot resonators for this type of sample is discussed in Section 7 of this chapter.

2.3 Reflection vs. Transmission Mode

Both transmission and reflection cavities have been utilized in high-field EPR applications. The earliest quasioptical spectrometers tended to rely more upon transmission cavities because of the simplicity of their construction, and because of the additional complications of constructing the quasioptical circuitry necessary to operate a reflection cavity. However, reflection cavities are intrinsically more sensitive than transmission cavities as Eqs. [2] show. For the reflection and induction cavities, sensitivity is optimized when the cavity is critically coupled, i.e., when $\beta=1$ and all incident power absorbed in the cavity. In this case, $M=1/2$. For a transmission cavity, sensitivity is optimized when $\beta_1=\beta_2=1/2$, so that half the power is absorbed in the cavity, one quarter is reflected, and one quarter transmitted. Under these conditions $M=1/8$. Thus, according to the FOM given in Eqs. [2], one might expect a reflection cavity to be four times more sensitive than a similar cavity operating in the transmission mode, assuming all other cavity characteristics could be kept equal.

In practice, such an advantage may be difficult to realize, since this analysis does not take into account other influences that both transmission and reflection cavities can have on spectrometer sensitivity. For example, the local oscillator (LO) power cannot be independently controlled in transmission mode, in the absence of an rf bucking scheme, which may limit the dynamic range of certain homodyne detectors. Similarly, complications can arise from the need to duplex the radiation that is incident upon and reflected from a reflection cavity. Adventitious reflections from quasioptics or the cavity can lead to significant standing wave problems that impede cavity tuning and can strongly impact the system sensitivity.

2.4 RF Magnetic Field

The power dissipated by the cavity can be written in terms of the input power as follows:

$$P_{diss} = C' P_0 \qquad [8]$$

where C' is a matching factor that depends upon the cavity configuration (transmission, reflection, or induction) as detailed below. Using the definition of unloaded cavity Q,

$$Q_U = \frac{2\pi(\text{energy stored in cavity})}{\text{energy dissipated per cycle}} = \frac{2\pi E_C}{E_{diss}} \qquad [9]$$

the dissipated power is simply E_{diss} divided by the cycle time,

$$P_{diss} = \frac{2\pi c E_C}{\lambda Q_U} \qquad [10]$$

The energy stored in the cavity can be calculated as

$$E_C = \frac{1}{2\mu_0}\int_{V_c} B_1^2 dV = \frac{V_C\langle B_C^2\rangle}{2\mu_0} = \frac{V_C\langle B_S^2\rangle}{2\mu_0 R_H} \qquad [11]$$

The unloaded cavity Q is related to the loaded cavity Q as follows for transmission, reflection, and induction cavities:

$$\begin{aligned} Q_{L,trans} &= \frac{Q_{U,trans}}{(1+\beta_1+\beta_2)} \\ Q_{L,refl} &= \frac{Q_{U,refl}}{(1+\beta)} \\ Q_{L,ind} &= \frac{Q_{U,ind}}{(1+\beta_1)(1+\beta_2)} \end{aligned} \qquad [12]$$

An expression for the average (root mean squared) mm-wave field at the sample, $\overline{B}_S \equiv \sqrt{\langle B_S^2\rangle}$ then follows from Eqs. [8] and [10]-[12]:

$$\overline{B}_S = \left[\frac{\mu_0\lambda Q_L C R_H}{\pi c V_C}\right]^{1/2} P_0^{1/2} \equiv K P_0^{1/2} \qquad [13]$$

where $C = C' Q_L/Q_U$ depends upon the cavity configuration as follows:

$$C_{trans} = \frac{4\beta_1}{(1+\beta_1+\beta_2)^2}$$
$$C_{refl} = \frac{2\beta}{(1+\beta)^2} \qquad [14]$$
$$C_{ind} = \frac{4\beta_1}{(1+\beta_1)^2(1+\beta_2)^2}$$

The proportionality constant K is tabulated for each cavity/sample geometry assuming critical coupling in the reflection mode in all cases.

2.5 Comparison of Cavities

To summarize the results of this section, the absolute and concentration sensitivity FOM are tabulated with the B_1 field proportionality factors defined above in *Table 2*. It should be noted that all of these quantities are scaled relative to the wavelength λ to facilitate comparison of different cavity types at a given frequency. Thus, in order to calculate an absolute value for N_{min} or N_{min}/V_S according to Eq. [1], it is necessary to divide by the indicated power of λ (in SI units), and similarly for calculating absolute B_1 field using Eq. [13].

Table 2. Comparison of figures of merit for different cavity configurations

Type	$F_A(\lambda^4)$			$F_C(\lambda)$		$K\ (T\,W^{1/2}\,\lambda) \times 10^{-6}$		
	Pt.	Cyl.	flat	Cyl.	flat	Pt.	Cyl.	flat
TE_{011}	1410	678	133	1	2	1.94	1.35	0.60
TE_{102}	1412	706	706	20	63	1.94	1.37	1.37
F-P	8.0	4.3	3.3	0.0025	0.025	0.15	0.11	0.094
Non	0.3	0.2	0.1	0.0001	0.1249	0.028	0.021	0.018

It is apparent from *Table 2* that single-mode cavities offer the best absolute and concentration sensitivity as well as the largest B_1 field for a given input power when compared to traditional Fabry-Pérot designs. However, at the very shortest wavelengths, fabrication of rectangular cavities with high Q factors are virtually unknown at these wavelengths. In contrast, single-mode cylindrical cavities have been fabricated at frequencies up to 360 GHz, and can offer over two orders of magnitude better sensitivity than open resonators for point and cylindrical samples. This advantage is less dramatic for the flat sample geometry. In fact, samples with very high dielectric losses typically must be

much thinner than the "flat" sample geometry assumed in *Table 1*, in which case, the FOM for cylindrical and Fabry-Pérot cavities become comparable. Reduced dimension Fabry-Pérot resonators (discussed above) may even surpass the performance of cylindrical cavities under otherwise similar conditions.

As *Table 2* also shows, single mode cavities afford the largest H_1 field for a given input power. This is mainly a consequence of their high Q factors and the relatively small cavity volumes, which tends to concentrate B_1 at the sample. Accordingly, the relatively low Q and large V_C of the typical Fabry-Pérot cavity assumed in *Table 1* make it very uncompetitive for pulsed applications in general. As we have discussed above, however, the Cornell group has recently employed a non-standard Fabry-Pérot resonator with $w \approx \lambda$ that addresses these shortcomings and leads to B_1 fields approaching those of cylindrical cavities for the same input power.

3. QUASIOPTICAL CAVITY COMPONENTS

Because of the flexibility of quasioptical design in EPR application, there are three distinct ways in which radiation may be introduced to the sample in a quasioptical EPR system: via (1) single-mode waveguide, (2) overmoded waveguide, or (3) free-space propagation as a Gaussian beam. We briefly review these methods of propagation as they pertain to cavity coupling.

3.1 Waveguide Propagation

At frequencies up to about 150 GHz, it has been possible to utilize conventional single-mode waveguide, which may be coupled to single-mode rectangular or cylindrical cavities, overmoded resonators (usually cylindrical), and even Fabry-Pérot resonators (Grinberg *et al.*, 1983; Burghaus *et al.*, 1992). However, at higher frequencies, transmission losses through single-mode waveguide become prohibitive for use with superconducting magnets where the length of guide can easily exceed 2 m. This has encouraged the use of overmoded waveguide, for which losses scale roughly as the inverse of the characteristic cross-sectional area L.

Overmoded smooth circular guide has been used at frequencies from 110 GHz up to 660 GHz (Müller *et al.*, 1989; Krzystek *et al.*, 1996) however, most groups now employ corrugated waveguide,(Smith *et al.*, 1995; Earle *et al.*, 1996b; Fuchs *et al.*, 1999; Hassan *et al.*, 2000; Smith and Riedi, 2000) which previously had found extensive use in plasma fusion experiments where it was necessary to propagate very high mm-wave power with very low loss on the order of 0.01 dB/m.(Doane 1985) Corrugated guide has lower transmission loss than smooth guide, and propagates a single hybrid HE_{11} mode (a linear combination of the TE_{11} and the TM_{11} modes) when excited by a Gaussian beam. This mode also maintains high polarization purity and is relatively

insensitive to distortions within the pipe, both of which are important for use with high-field EPR cavities.

Waveguides, both corrugated and smooth, may be connected to the sample holder or EPR cavity in a number of ways. Non-resonant sample holders may be placed directly in the waveguide, or inside of small gaps between waveguides. Corrugated waveguides produce a nearly Gaussian beam at the output (see next section, 3.2), and may therefore be coupled directly to the Gaussian beam in an open resonator, or to quasioptical components. Alternatively, a conical horn or taper (section 3.3 below) may be used to convert the radiation to single-mode waveguide, which may then be introduced into the cavity by waveguide coupling methods.

3.2 Gaussian Beam Propagation

Another method for introducing radiation into a quasioptical sample cavity is free-space propagation of a Gaussian beam (Goldsmith 1982; Goldsmith 1998), which is illustrated in *Figure 1*. The electric field intensity follows the dependence exp $(-\rho^2/w^2)$, where ρ is the radial distance from the direction of propagation, and w is a position-dependent parameter governing the radius of the field distribution. A fundamental Gaussian beam is completely characterized at a given frequency by the beam-waist w_0, which corresponds to the $1/e$ width at the narrowest part of the beam. The beam radius w at some distance of propagation z away from the beam waist will be

$$w = w_0\left[1+\left(\frac{z}{z_R}\right)^2\right]^{1/2} \qquad [15]$$

and the radius of curvature R at a distance z from the beam waist is given by

$$R = z\left[1+\left(\frac{z_R}{z}\right)^2\right] \qquad [16]$$

where z_R is the Rayleigh length (also called the *confocal distance*) given by $w_0{}^2 / \pi\lambda$.

Gaussian beam propagation has been used by some groups to transmit mm-waves over a significant distance via a series of lenses separated by the sum of their focal lengths.(Lynch *et al.*, 1988; Budil *et al.*, 1989; Cardin *et al.*, 1999)

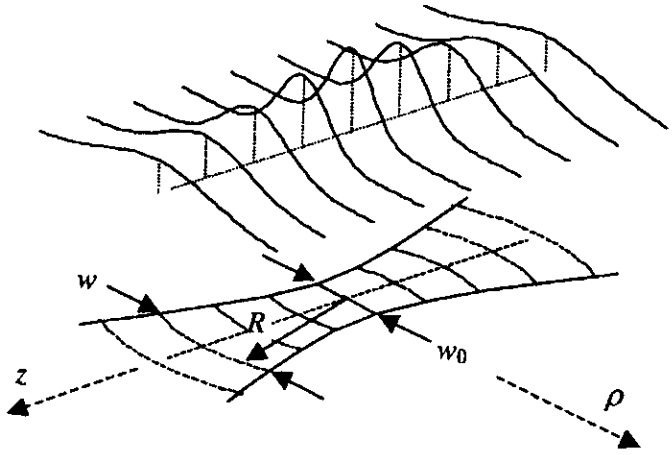

Figure 1. Parameters of a Gaussian beam

In such systems, the beam may be introduced directly into the sample cavity by passing it through a partially reflective mirror.(Lynch *et al.*, 1988; Budil *et al.*, 1989; Cardin *et al.*, 1999; Rohrer *et al.*, 1999) A free-space Gaussian beam may also be launched from an overmoded waveguide by passing the radiation through an appropriate taper section attached to the guide. (Earle *et al.*, 1996b; Smith *et al.*, 1998)

3.3 Conical Horns and Tapers

Conical horn antennas and conical tapers are very important for cavity design because they allow interconversion between overmoded circular waveguide and either single-mode waveguide or a Gaussian beam with very low insertion loss (typically < 0.25 dB). Thus, it is possible in principle to match different cavity designs with the different propagation methods that may be employed by the spectrometer. Examples of their application are depicted in *Figure 2.*

There is a rather large literature on the design, fabrication, and modeling of corrugated horns, which have found widespread use in radar systems.(Goldsmith 1982; Goldsmith 1998) Conical horns most typically use corrugations to improve mode matching and polarization characteristics. They are usually manufactured by electroforming copper on an aluminum mandrel and then etching away the aluminum, although corrugated conical sections may be machined directly in some cases. It has been shown that horns with narrow flare angles (typically less than 5°) convert the TE_{10} mode to a fundamental Gaussian mode with >98% efficiency; the

Gaussian output beam has a waist $w_0 = 0.6345a$, where a is the aperture radius of the horn.(Wylde 1991)

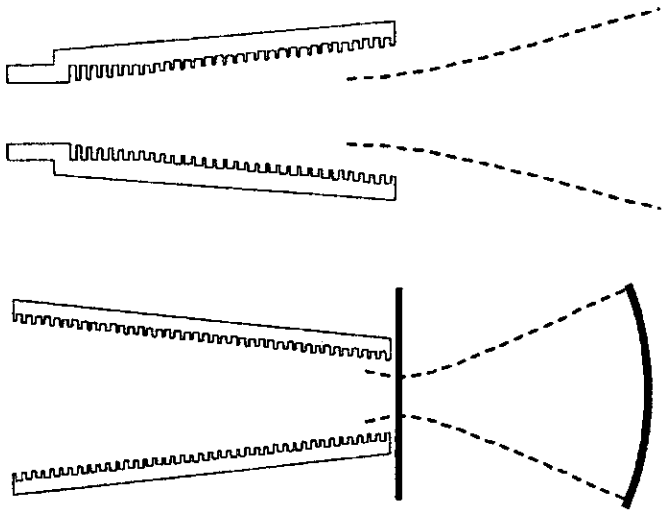

Figure 2. Scalar conical horn antenna (a) coupling to a Gaussian beam, and conical taper (b) coupling into a semiconfocal Fabry-Pérot cavity.

The distance from the aperture to the beam waist is

$$z = \frac{R_a}{1+\left[\lambda R_a/\pi(0.6435a)^2\right]^2} \qquad [17]$$

and the beam waist is given by

$$w_0 = \frac{0.6435a}{1+\left[\dfrac{\pi(0.6435a)^2}{\lambda R_a}\right]} \qquad [18]$$

where z is the distance from the beam waist to the horn aperture, R_a is the radius of curvature of the beam at the aperture (equal to the slant length of the feed horn), and a is the aperture radius. For a cone half-angle of θ, we have

$\sin\theta = a/R_a$. Eqs. [17] and [18] can be applied to either the larger or the smaller aperture of a conical taper using the convention that $R_a < 0$ at the larger end. Thus, at the larger end of a taper, by analogy with a horn antenna, the effective beam waist is some small distance inside the horn; at the smaller end of a (truncated) conical feed, the beam waist is projected a small distance outside the horn. When θ is sufficiently small, it is possible to broadcast the mm-waves directly from the horn into a Fabry-Pérot cavity mode.

3.4 Focusing Elements

Occasionally, coupling between either waveguide or free-space modes of propagation and an open cavity has been achieved via a coupling lens, which is usually fabricated from a dielectric material with grooves cut in the surface to make an artificial quarter-wavelength matching layer.(Jones and Cohn 1955) The grooves significantly reduce the power reflected by the lens. Off-axis mirrors are generally preferable to lenses as focusing elements in mm and sub-mm wave instrumentation where performance is critical, but they are typically not used in cavity design because of space considerations. Lenses have the advantage of compactness and ease of manufacture, but generally offer worse performance than mirrors in terms of astigmatic amplitude, insertion loss, standing waves, cross-polar effects, and limited bandwidth. For example, the insertion loss of a feed horn–lens configuration is about 1dB at 90 GHz, and increases at higher frequencies. This disadvantage is frequently offset by the compactness of a coupling lens, which offers the flexibility of switching between waveguide-based cavities and open cavities as needed.

3.5 Beam splitters

Although freestanding wire grid polarizing beam splitters are essential components of the circuitry in quasioptical EPR spectrometers, they are not used in cavities for a number of reasons. (A closely related structure, the polarizing mirror, can be incorporated into the cavity design as described in the next section). However, several of the more elaborate reflection cavity designs in the literature do use nonpolarizing beam splitters in the form of a sheet or slab of dielectric material such as Mylar. Such beam splitters are most typically used as power dividers (or –3 dB couplers) with an incident angle of $\pi/4$.

Since the reflection coefficients of a dielectric slab for vertical and horizontal polarizations are in general quite different, simple division of power without complicating phase effects can only be achieved when the input polarization is either parallel or perpendicular to the plane of incidence, with vertically polarized input (perpendicular to the plane of incidence) most typically utilized and the thickness of the dielectric is adjusted to give the desired reflection and transmission coefficients for this polarization. One can

construct a −3 dB coupler for a reasonably broad frequency range by choosing a dielectric with an appropriate permittivity ε (see (Goldsmith 1998) for details) and adjusting the thickness to a half-wavelength.

3.6 Partially Reflective Mirrors

Many cavities in current use are based on partially reflective mirrors. The most common application utilizes a planar, partially reflective mirror in conjunction with a spherical mirror to form a semiconfocal Fabry-Pérot resonator. The planar mirror is placed as near as possible to the beam waist of the Gaussian beam mode that is set up in the cavity. The main advantage of this type of arrangement is that incident Gaussian beams may be aligned with the fundamental cavity mode and directly coupled into the cavity, greatly improving the coupling and avoiding losses due to mode mismatch, mode conversion, and scattering that are associated with other coupling elements such as irises.(Matsui *et al.*, 1993).

Figure 3 depicts the most common kind of nonpolarizing mesh utilized in quasioptical EPR cavities, a so-called "inductive" mesh of flat conducting wires. The most important grid parameters that determine mirror reflectivity at a given frequency are the grid spacing g and the width of the wires $2a$. Most of the earlier cavity designs used free-standing, electroformed meshes of flat Cu, Ag, or Au wire approximately 50 μ in thickness with 40-100 wires cm^{-1}, commercially available from Buckbee-Mears (St. Paul, MN).

However, there are several problems in the application of commercially available meshes to quasioptical EPR. The first major difficulty is that freestanding meshes are significantly affected by Lorentz forces that arise from the 1-100 kHz modulation field used in cw-EPR. The resulting motion of the mirror can lead to large offset signals in the lock-in amplifier, significantly deteriorating the dynamic range and the signal-to-noise ratio of the EPR signal.

The most common approach to reducing the mesh motion has been to fix it to a suitable flat dielectric support surface. This solution has proved unsatisfactory for a number of reasons. It is rather difficult to achieve a thin and even coating of adhesive that allows the mesh to be applied flat, and even very thin layers of adhesive in the active area of the mirror can significantly affect its performance. Such difficulties can be avoided by using adhesive only around the edge of the dielectric window, or by holding the mesh against the window with tension (Ulrich 1967) but this leaves the mesh very susceptible to breaking at lower temperatures due to the different expansion coefficients of the metal and dielectric.

A second significant difficulty is that the wires in commercially available meshes are rather thin, which leads to a significant frequency dependence of the mesh's effective reflectivity. In multifrequency spectrometers, it therefore becomes necessary to change the sample cavity mirrors in order to achieve comparable performance at different wavelengths.

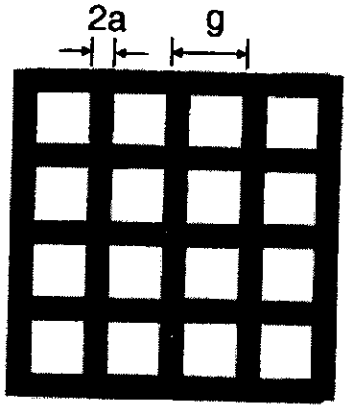

Figure 3. Schematic diagram of resonant inductive mesh

The frequency dependence of inductive grids can be understood in terms of its characteristic transmission line impedance Z_g (Marcuvitz 1951). For a grid of flat, perfectly conducting wires sandwiched between two different dielectric materials, the effective impedance is given by (Goldsmith 1998)

$$\frac{Z_g}{Z_0} = j\omega_0'\left(\frac{g}{\lambda}\right)\ln\csc\left(\frac{\pi a}{g}\right)\left[\frac{\omega}{\omega_0}-\frac{\omega_0}{\omega}\right]^{-1} \qquad [19]$$

in which $\omega = g/\lambda$ is the reduced frequency, and

$$\omega_0' = \omega_0\left(\frac{2}{n_1^2+n_2^2}\right)^{1/2} \qquad [20]$$

where the two dielectric layers have refractive indices n_1 and n_2, respectively, and ω_0 is a dimensionless empirical parameter that models the observed resonant property of inductive meshes, typically about 0.80-0.85 in value.

The resonant behavior of inductive meshes is responsible for the frequency dependence in their reflectivity. The sharpness of the resonance depends strongly on the $g/2a$ ratio that describes the grid proportions, as illustrated in *Figure 4*. Values of $g/2a < 2$ produce a much sharper resonance near ω_0', which is accompanied by a relatively broad range of frequencies over which the mesh reflectivity is essentially constant. Unfortunately, commercially available

meshes have $g/2a$ ratios that are more typically 5 or greater, leading to appreciable frequency dependence of the reflectivity. Thus, commercial meshes are less suitable for application in the more recent broadband and multifrequency quasioptical EPR bridge designs.

Several groups have recently introduced alternatives to the electroformed meshes that significantly improve the bandwidth, performance and durability of meshes for use in EPR cavities. The Cornell group has recently fabricated mirrors using Cu foil and commercial photo-etching kit such as is used to fabricate circuit boards. Since the smaller $g/2a$ ratios require larger values of g and a to produce a given reflectivity in the 0.5-3 mm wavelength range, the resulting patterns are large enough that the template for the photo mask can be produced on a standard 600 dpi laser printer with reasonable accuracy. Care must be taken to select g and a values that are integer multiples of the printer resolution to avoid moiré effects on the printed pattern. This procedure produces a relatively thick, durable metal mesh that is far less susceptible to Lorentz forces and the physical demands of mounting the mirror in the cavity.

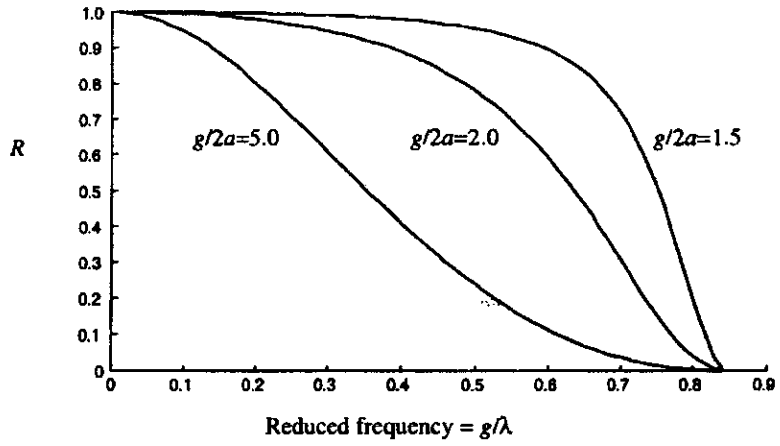

Figure 4. Reflectivity vs. reduced wavelength for different $g/2a$ ratios. Note the broad region of nearly constant reflectivity in the curves at lower values of $g/2a$.

A grid pattern with appropriate $g/2a$ ratio can also be deposited photolithographically onto a suitable substrate such as a quartz window using standard microfabrication techniques. This arrangement can provide even greater mechanical stability and better handling than the free-standing foil, although the metal thickness deposited using such methods is typically much

less than the skin depth at mm-wave frequencies, leading to higher resistive losses in the conductor. Such difficulties may be avoided by electroplating additional metal onto the deposited pattern, which can be accomplished to a thickness of 2 μm or more without significant distortion of the pattern.

An additional complication with dielectric-backed meshes is that the dielectric support can also act as a planar Fabry-Pérot interferometer because of the partial reflections from the dielectric discontinuities at the window surfaces. Thus, care must be taken in designing the support thickness. With a little forethought, it is possible to design the dielectric support so as to have high reflectivity over the frequency range corresponding to the resonant transmission "dip" of the metal grid, thus extending the bandwidth over which a given design reflectivity applies. The matrix method presented in Section 7 may also be used to calculate the reflectivity of a given mirror-dielectric combination for design purposes.

4. QUASIOPTICAL INDUCTION MODE CAVITIES

Since a number of recently constructed quasioptical EPR spectrometers operate with induction mode cavities, it is worthwhile to devote some attention to how this type of cavity is characterized. Induction-mode EPR was described in 1961 by Teaney *et al.* (1961), but did not enjoy very widespread application in waveguide-based spectrometers, perhaps because of the difficulties in constructing the appropriate bimodal cavity that is required (Portis and Teaney, 1958). At quasioptical frequencies, induction spectroscopy has been applied in transmission cavities at 130 GHz, and introduced to reflection cavities by the groups of Freed (Earle *et al.*, 1996a,b) and Smith (Smith *et al.*, 1998).

The advantage of quasioptical cavities for induction mode spectroscopy is that the same physical entry point may be used as both an input and an output port if polarization encoding is employed. In this case, the polarization states distinguish the cavity input and output ports, and the cavity can be considered to be bimodal. Since quasioptical polarizers offer excellent isolation between perpendicular linear polarizations, there is no need for an isolator between cavity and detector, which greatly improves the system noise figure. Quasioptical induction mode cavities are also easily scaleable with frequency.

The properties of induction mode cavities are best understood in terms of the Jones matrix representation, which is a useful analytical method for describing a wide variety of different quasioptical systems.(Lesurf, 1990) This formalism is analogous in some ways to the standard equivalent circuit (Poole, 1983) and transmission line models (Wilmshurst *et al.*, 1962) used to describe waveguide-based EPR spectrometers, except that it takes explicit account of the polarization state of the radiation. The polarization state is expressed in terms of a column 2-

vector representing the mm-wave E fields in the vertical and horizontal directions, for which some important special cases are shown in *Figure 5*.

Jones matrix representations for transmission and reflection mode EPR sample resonators have been derived by Budil *et al.*, 2000 and are reproduced in *Table 3*. These representations embody a number of important properties required for a quasioptical cavity to operate effectively in induction mode. Most importantly, the cavity must have cylindrical symmetry; that is, the same Q and coupling factors for two orthogonal linear polarizations. In this case, the reflected or transmitted EPR signal is circularly polarized, and circularly polarized incident radiation may be coupled directly into the cavity. This requirement limits the types of single-mode cavities that can be practically used in induction mode spectroscopy to end-coupled cylindrical cavities and open resonators.

$$\underset{\text{vertical}}{\begin{pmatrix} E_0 \\ 0 \end{pmatrix}} \quad \underset{\text{horizontal}}{\begin{pmatrix} 0 \\ E_0 \end{pmatrix}} \quad \underset{\text{circular}}{\begin{pmatrix} E_0/2 \\ \pm iE_0/2 \end{pmatrix}}$$

Figure 5. Vector representations of different mm-wave polarization states in the Jones matrix formalism.

A second, related feature implicit in these representations is that the cavity does not introduce any coupling between the two polarization modes other than the EPR signal itself, although one could model cross-coupling effects in a straightforward way with Jones matrices containing off-diagonal entries similar to those given in *Table 3*, but independent of χ.

Table 3. Jones matrix representations of quasioptical transmission and reflection cavities

Transmission	$\dfrac{\sqrt{\beta_1\beta_2}}{(1+\beta_1+\beta_2)}\begin{pmatrix} 1-i\eta Q_L\chi & \eta Q_L\chi \\ -\eta Q_L\chi & 1-i\eta Q_L\chi \end{pmatrix}$
Reflection	$\dfrac{(1-\beta)}{(1+\beta)}\begin{pmatrix} 1+\dfrac{\beta}{(1-\beta)}i\eta Q_L\chi & \dfrac{\beta}{(1-\beta)}\eta Q_L\chi \\ -\dfrac{\beta}{(1-\beta)}\eta Q_L\chi & 1+\dfrac{\beta}{(1-\beta)}i\eta Q_L\chi \end{pmatrix}$

4.1 Transmission Mode

To illustrate the use of a transmission cavity in induction mode, we form the simple matrix-vector product representing the interrogation of a perfectly matched sample-containing cavity by a vertically polarized mm-wave beam:

$$\frac{1}{4}\begin{pmatrix} 1-i\eta Q_L\chi & \eta Q_L\chi \\ -\eta Q_L\chi & 1-i\eta Q_L\chi \end{pmatrix}\begin{pmatrix} E_0 \\ 0 \end{pmatrix} = \frac{E_0}{4}\begin{pmatrix} 1-i\eta Q_L\chi \\ -\eta Q_L\chi \end{pmatrix} \qquad [21]$$

This output beam is the superposition of a vertically polarized "carrier" and a circularly polarized EPR signal proportional to $\eta Q_L\chi$ (*cf. Figure 5*). To utilize such a cavity in induction mode, one would place a horizontal polarizer in front of the cavity so that only the EPR signal is "seen" by the detector. This feature is particularly useful in pulsed applications where the detector must be protected from high input power, and polarizing grids offer excellent isolation between the two linear polarizations.

Budil *et al.* (2000) have demonstrated that this arrangement also affords phase discrimination of the EPR signal when used with a homodyne detector, since the effective phase lag between the carrier (which functions as the local oscillator) and the circularly polarized signal can be controlled by varying the angle of the polarizer or input waveguide. Explicitly, the detected signal can be expressed as

$$\begin{aligned} |E_\theta|^2 &= a_T^2\cos^2\theta \\ &+ a_T b_T\left[(\cos 2\theta + 1)\chi''^{(1)} - \sin 2\theta\chi'^{(1)}\right]\sin\omega_m t \\ &+ b_T^2\left[\left(\left(\chi'^{(1)}\right)^2 + \left(\chi''^{(1)}\right)^2\right)\right]\sin^2\omega_m t \end{aligned} \qquad [22]$$

where θ is the angle of the polarizer with respect to the vertical, ω_m is the field modulation frequency, and a_T and b_T are constants. The first, time-independent term represents the transmitted source power at the detector, which exhibits the expected $\cos^2\theta$ dependence upon the detector orientation. The $\sin(\omega_m t)$ term detected by a lock-in amplifier contains both absorption and dispersion terms, which are weighted according a half-angle relationship between the detector angle and the effective phase of the spectrum. Thus, it is possible to observe a pure absorption signal, but not a pure dispersion signal.

4.1.1 Reflection and Induction Modes

Figure 6 show two quasioptical circuits that represent the simplest possible implementation of a reflection cavity in a quasioptical homodyne detection system. In such systems, a fraction of the source power is diverted into a reference arm with an adjustable path length. For the simple systems shown in *Figure 6*, this may be accomplished by splitting the beam with a polarizing wire grid, and utilizing a rooftop mirror in the reference arm to rotate the polarization of the reflected mm-waves by an angle of $\pi/2$ so that it passes back through the grid to the detector. The phase of the reference signal is adjusted by changing the position of the rooftop mirror.

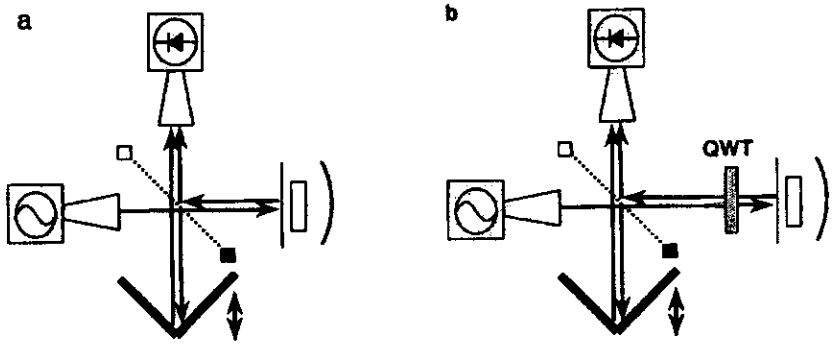

Figure 6. Two greatly simplified schemes illustrating the application of a reflection cavity in quasioptical spectrometers: (a) induction mode and (b) polarizing interferometer mode.

Much more sophisticated reflection mode configurations based on quasioptical Faraday rotators have been described in which the signal and reference beams are physically separated (Smith *et al.*, 1998; Smith and Riedi, 2000), affording better control over signal phase and stray reflections. However, the simple designs shown in *Figure 6* do serve to illustrate the requirements for cavities in this type of system. *Figure 6a* shows an induction mode spectrometer in which the sample is irradiated with linearly polarized mm-waves and a circularly polarized EPR signal emerges from the cavity. Only one linearly polarized component is reflected from the grid into the detector, where it is mixed with the referenced signal. The most important feature of the induction mode arrangement is that power reflected from the cavity does not appear in the

induction mode signal, in the absence of cross-coupling terms. This greatly reduces possible signal degradation due to modulation of the cavity parameters.

The polarizing interferometer design shown in *Figure 6b* is nearly identical, but includes a quarter-wave transformer (QWT) between the sample arm and the polarizing grid. Although a dielectric quarter-wave plate can be used in this capacity, most practical broadband implementations of the polarizing interferometer scheme utilize either a polarization-transforming reflector (Earle *et al.*, 1996a,b) or a Martin-Puplett interferometer (Smith *et al.*, 1998; Smith and Riedi, 2000) to accomplish the quarter-wave transformation.

The QWT has two effects: first, the incident radiation is converted to circular polarization, effectively doubling the mm-wave power at the sample (assuming the circular polarization is the correct one for the given sign of electronic g factor). Secondly, the circularly polarized EPR signal is converted to a linear polarization before being reflected into the detector, so that all of the signal power can in principle be utilized. Despite this apparent advantage, imperfections in the quarter-wave transformation and adventitious standing waves between cavity and QWT can offset these advantages, and better isolation between EPR signal and input power offered by the induction design is often preferable.

5. SURVEY OF HIGH-FIELD CAVITIES

5.1 Non-resonant Sample Holders

A common sample treatment, particularly in the earliest high-frequency spectrometers,(Müller *et al.*, 1989) has been to place the sample in a non-resonant holder. Typically the holder is fabricated from a dielectric material with a cylindrical well that holds the sample between two windows in the beam path of a transmission spectrometer, usually in a small gap between cylindrical wave guides. More recent applications utilize a cylindrical metal "sample bucket" that functions essentially as a short length of smooth-walled cylindrical waveguide directly attached to the input waveguide and placed against a flat mirror for use in a reflection spectrometer.

The major advantage of non-resonant sample holders is that they work over a very wide range of frequencies (Hassan *et al.*, 1999; Hassan *et al.*, 2000) and are thus a natural choice for samples in broadband multifrequency studies. A second significant advantage of non-resonant bucket designs is that they afford considerably simpler sample handling and loading than sample resonators.

Because there is no amplification of the mm-waves at the sample, non-resonant devices have very low absolute sensitivity compared to sample resonators. Nevertheless, they can also provide reasonably good concentration sensitivity for low loss powders, liquids, and frozen samples, where it is possible

to fill the non-resonant structure with sample, so that the effective $Q\eta$ product remains high. Non-resonant holders may also have some advantages for certain types of large-grain powders, where large sample volumes may be required to average out polycrystalline effects (Poolton *et al.*, 2000). Non-resonant systems may also be effective for high loss samples such as thin films, or samples in which the losses are dominated by magnetic effects (as opposed to dielectric losses). Finally, such sample holders are less susceptible to saturation effects because of the low B_1 field, and may be useful in spectrometers where it is inconvenient to attenuate the source power reproducibly.

A number of difficulties have been encountered with non-resonant bucket sample holders, particularly in the transmission mode. Inevitably there are reflections from the surfaces of the sample holder that can increase radioactive losses or lead to standing waves that interfere with signal detection. Mode conversion in the bucket or surrounding waveguide can also produce admixtures of absorption and dispersion signals. The inability to control the carrier power independently of the signal power at the detector can also saturate the detector. Some of these problems can be circumvented by employing an induction spectrometer design with a non-resonant holder.(Smith *et al.*, 1998)

5.2 Single Mode Cylindrical Cavities

Single mode cylindrical cavities have become standard in waveguide-based EPR spectrometers at frequencies up to 140 GHz.(Brezgunov *et al.*, 1991; Burghaus *et al.*, 1992; Becerra *et al.*, 1995; Disselhorst *et al.*, 1995) A single-mode resonator with $Q_L \approx 3000$ is available for use with the commercial Bruker 95 GHz spectrometer (Schmalbein *et al.*, 1999) and this is typical of many W-band single-mode cavities that had previously been described in the literature.

Cylindrical cavities have the advantage that they can be designed with reasonably high Q as well as very large filling factors, so that they typically afford the maximum mm-wave B_1 field for a given input power. As *Table 2* shows, such cavities can offer several hundred times better sensitivity than standard Fabry-Pérot resonators. This also makes them desirable for pulsed methods that require the largest possible B_1 field, such as time-domain EPR and pulsed ENDOR (Prisner *et al.*, 2001) and dynamic nuclear polarization (DNP) (Becerra *et al.*, 1995). Weis *et al.* (1999) have recently described a special cavity for high-field DNP and ENDOR at an EPR frequency of 140 GHz that consists of a flat helical wire wound into a structure that functions as a cylindrical TE_{011} cavity. The helical structure permits irradiation of the sample with ^1H and ^{13}C nuclear frequencies.

Cylindrical cavities have also been designed for fairly wide-band performance. Hill *et al.* (1999) have reported a tunable TE_{01p} cylindrical cavity operating in transmission mode from 30 to 120 GHz. The group at Grenoble (Seck and Wyder, 1998) has reported a continuously tunable wide band single-mode cavity operating from 40-60 GHz in reflection mode for EPR and ENDOR

applications. The coupling is adjusted by moving a Teflon tuner positioned just above the cavity hole, and the reported Q_L varied from 4000 at 40 GHz to 1000 at 60 GHz.

Among the disadvantages of single-mode cylindrical cavities is that they may be difficult to manufacture because of their relatively small size in comparison to the radiation wavelength. Until recently, there had been a common perception that the upper limit on frequencies at which such resonators could be applied coincided with the practical upper limit for waveguide-based technology, or about 140 GHz.

Nevertheless, the excellent performance of single-mode resonators at or below 140 GHz has spurred researchers to develop similar devices at even higher frequencies. There have been recent reports of single-mode cylindrical cavities operating at 180 GHz with a Q of several thousand,(Rohrer *et al.*, 2001) at 270 GHz with Q_L = 1000 (Smith and Riedi 2000), and most recently at 360 GHz (Disselhorst and Schmidt 2000). These initial efforts suggest that cylindrical cavities with reasonably high Q can be designed and fabricated even at very high frequencies. These developments may greatly extend the frequency range over which cylindrical cavities significantly outperform Fabry-Pérot resonators, for which the reported finesse values have often been disappointingly low compared with the theoretical maximum.

It is not yet clear what the practical frequency limit may be for the application of cylindrical cavities. This is further support for the authors' position that there is a broad frequency range over which waveguide and optical techniques may be used. Ultimately, the dimension of the sample capillary tube may impose the final constraint, particularly for low-concentration samples requiring a large volume.

5.3 Fabry-Pérot Interferometers

Quite a number of high-frequency EPR spectrometers have been based on variations of the basic Fabry-Pérot interferometer (FPI), (Lynch *et al.*, 1988; Barnes and Freed 1997; Smith *et al.*, 1998; Cardin *et al.*, 1999; Fuchs *et al.*, 1999; Moll *et al.*, 1999; Rohrer *et al.*, 1999). In practical applications, FPIs have been constructed from two spherical mirrors (confocal arrangement) (Haindl *et al.*, 1985), or a combination of one planar and one spherical mirror (semiconfocal arrangement) (Lynch *et al.*, 1988; Budil *et al.*, 1989). It is also possible to form a resonator from two partially reflective planar mirrors, although this arrangement is not typically used in EPR applications. Nevertheless, some of the design principles discussed below implicitly utilize the interferometric properties of a planar window-sample-window arrangement.

The wide appeal of the Fabry-Pérot resonator for high-field EPR is attributable to a number of features. The performance of Fabry-Pérot devices in the millimetre-wave regime has also been extensively characterized in other contexts (Clarke and Rosenberg 1982), so that there was a large pre-existing

knowledge base for EPR applications. The design is quite compatible with systems based on Gaussian beam optics, and semiconfocal resonators permit direct coupling of a beam into the cavity. Particularly important is the cylindrical symmetry of the Fabry-Pérot resonator, which makes it useful in simple induction-mode designs, as well as a number of detection schemes that utilize polarization-encoding schemes that require the cavity to support circular polarization.

Open resonators are quite flexible, and can accommodate enhancements such as optical illumination for studying photosynthetic systems (Möbius, 2000), crystal rotation (Earle and Freed, 1999), application of rf fields for ENDOR (Burghaus *et al.*, 1988) and field-jump coils for stepped-field ELDOR and similar classes of experiments. Finally, reasonably high Q values can be attained with Fabry-Pérot resonators for a broad range of sample characteristics, including high-loss aqueous samples as discussed below. This feature makes the Fabry-Pérot resonator attractive in cases where absolute sensitivity is an important criterion.

The important figure of merit for Fabry-Pérot resonators is not the cavity Q, but rather the finesse $\mathcal{F} = Q/m$, where m is the number of half-wavelengths between the mirrors. The theoretical upper limit for the cavity finesse is determined by the resistivity of the metal in the mirrors, and is about 1600 at 100 GHz and about 900 at 300 GHz for gold. In practice, additional resistive losses in mirror mesh material, imperfect coupling to the principal cavity mode, and scattering from the mirrors or irises becomes significant. As *Table 4* shows, most reported practical EPR implementations of the Fabry-Pérot resonator have a finesse that is considerably smaller than the theoretical maximum.

Another potential disadvantage of conventional Fabry-Pérot resonators is that their effective volume is much larger than that of a single mode cavity. The delocalization of the mm-wave field energy over the cavity volume generally leads to a smaller B_1 field for a given power.

Table 4. Reported Fabry-Pérot resonator finesse for existing quasioptical EPR spectrometers as a function of frequency

Frequenc y	Finesse	Ref
90	500	(Smith *et al.*, 1998)
110	80	(Rohrer *et al.*, 1999)
180	260	(Smith *et al.*, 1998)
220	40	(Rohrer *et al.*, 1999)
270	180	(Smith *et al.*, 1998)
330	30	(Rohrer *et al.*, 1999)
360	130	(Fuchs *et al.*, 1999)
600	40	(Moll *et al.*, 1999)
250	50	(Earle *et al.* 1996)
170	40	(Earle *et al.*, 1996)
220	40	(Cardin *et al.*, 1999)

In addition to losses from the mirrors or coupling elements, Fabry-Pérot cavities are also susceptible to irradiative losses from the sample cavity, including scattering by the sample, and aperture effects. Irregularly shaped or highly scattering samples can severely limit the performance of Fabry-Pérot resonators, and performance is by far the best for planar samples. It has proved possible to mount tubes containing liquid samples transversely in Fabry-Pérot cavities in cases where the tube dimension is either much larger (Budil *et al.*, 1993) or much smaller than the irradiating wavelength; van Tol (2002) has reported good sensitivity with aqueous samples in transverse capillaries about 100μm in diameter.

Aperture effects are related the so-called "edge taper" of Gaussian beams,(Goldsmith 1998) which can be used to define the fraction of the beam power that is included within a finite aperture. An aperture with a radius $r = 1.5w$ will transmit about 98% of the power in a fundamental Gaussian beam, and one with $r = 2w$ will transmit 99.99% of the power. Because of the multiple reflections in a resonator, the radius r of a Fabry-Pérot mirror must typically be at least $2.5w$ before diffraction losses due to aperture effects become smaller than the resistive losses in the mirrors. (Goldsmith 1998) The requirement of a large aperture makes the mirrors somewhat bulky and difficult to operate in a cryostat, and if the mirrors are manufactured from metal, their size can also lead to significant eddy current losses in the modulation field.

At higher $\mathcal{F}$ values, the Fabry-Pérot cavity also requires more exacting mechanical tuning of the mirror separation, which renders the cavity tune highly sensitive to small temperature fluctuations and vibrations. Another difficulty with high finesse resonators is that they may require a means of adjusting the coupling in order to accommodate for samples of different dielectric loss properties. The simplest implementations of the Fabry-Pérot resonator have not allowed for variable coupling, although several advanced resonator designs are now available which do provide this flexibility, as discussed below.

Radiation may be coupled into a simple Fabry-Pérot cavity either through apertures in the mirrors, or by making one or both mirrors partially reflective. The first such resonators applied in high-field EPR utilized coupling apertures. (Grinberg *et al.*, 1983; Haindl *et al.*, 1985; Lynch *et al.*, 1988) A convenient approximation for the aperture diameter d at critical coupling is $d = \lambda/3$, where λ is the radiation wavelength.(Goy 1983) More typically, a significantly larger aperture has been used. At 250 GHz, large coupling apertures were used in order to accommodate a wide variety of sample types in the cavity.(Lynch *et al.*, 1988) Under these conditions, the cavity Q_L is dominated by irradiative losses, i.e., $Q_L \approx Q_R << Q_U$ and the cavity becomes quite insensitive to the contribution of sample dielectric loses to Q_U.

In practical applications, the sample should be placed as close as possible to the beam waist in the cavity in order to maximize the H_1 field at the sample. A resonant mode should be selected that avoids confocal separation of the mirrors (i.e., with each spherical mirror placed at distance z_C from the cavity beam

waist). At this particular mirror separation, many of the resonator modes are degenerate, which may lead to significant losses due to mode conversion. Operation of the resonator away from the confocal separation eliminates such losses by exploiting the dispersive character of the resonant modes.

5.4 Variable-coupling Cavities

In an ideal system, there is effectively no signal from the cavity away from an EPR resonance. This is achieved either by using some type of bimodal cavity with perfect isolation between the modes, or by perfectly matching the cavity to the EPR bridge. Thus, a means of matching the resonator to the rest of the spectrometer circuit is highly desirable in quasioptical systems, just as in waveguide-based systems.

At conventional microwave frequencies, coupling is most commonly achieved by mechanically changing the effective size of the coupling hole. At 94 GHz, it proved possible to use an oversized aperture and vary the coupling for different sample types by using a sliding dielectric wedge in front of the coupling aperture.(Haindl *et al.*, 1985) At higher frequencies, such a scheme becomes impractical due to the small dimensions of the required waveguide discontinuities and one is restricted to substitution of mirrors with different aperture diameters for coarse tuning. However, a number of alternative strategies have evolved that permit more flexible, continuous tuning of the coupling for basic Fabry-Pérot resonators.

5.4.1 Polarizing Cavity Mirror

Another approach to variable coupling in a Fabry-Pérot cavity is to utilize a polarizing reflector for one of the mirrors. The effective reflectivity of this mirror is then adjusted by rotating the polarization direction relative to the polarization of the input beam. The performance of such a cavity has been analyzed by Reijerse *et al.* (1998) and Budil *et al.* (2000). The analysis shows that the signal measured perpendicular to the polarization of the incident beam is obtained with sensitivity proportional to $(Q_L)^{1/2}$, where Q_L is derived from the coupling parameter for the mirror in the co-polar direction. The corresponding Jones matrix for this case may be derived by analogy with the equivalent circuit analysis given by Portis and Teaney 1958,

$$\mathbf{C}_R = \begin{pmatrix} i\dfrac{\beta Q_L}{(1+\beta)}\eta\chi & \left(\dfrac{\beta Q_L}{1+\beta}\right)^{1/2}\eta\chi \\ -\left(\dfrac{\beta Q_L}{1+\beta}\right)^{1/2}\eta\chi & -i\eta\chi \end{pmatrix} \qquad [23]$$

in the frame where the incident beam is polarized along the vertical direction. Such a cavity should be useful in time-domain spectrometers where it is desired to isolate the detection circuitry from high-powered source pulses. At the moment, freestanding wire-grid polarizers, or more specifically the required tensioning frames, are too bulky to permit easy implementation of this technique at high fields. A wire grid deposited on a dielectric substrate, by analogy to the meshes described in section 3.6, would be the most useful device for a practical implementation of this scheme.

5.4.2 Interferometric Coupling

Another means of varying the coupling is to use an adjustable interferometer. At 250 GHz, this technique is the quasioptical analogue of the common X-band practice of tuning a resonator by mechanically varying the effective impedance of the resonator iris to provide optimum coupling for a given sample. In the quasioptical case, the effective impedance is varied by changing the spacing between two thin sheets of Mylar, which has low losses at these frequencies. The transmission line equations suitable for analyzing a quasioptical circuit, where the symmetry axis of the interferometer is parallel to the optical axis may be written down using the transfer matrix formalism discussed in Section 7.

5.4.3 Shunt Cavities

Barnes and Freed have developed a unique Fabry-Pérot resonator at 250 GHz that is designed to accommodate a thin, disc-shaped sample with the normal to its flat surface perpendicular to the field direction. This geometry is specifically designed for ordered aqueous samples such as membranes or fibers, where it is desirable to study the sample at the canonical field orientations of 0° and 90° with respect to the ordering axis of the sample. As in the simple transmission cavity, aqueous samples must be carefully placed at an *E*-field node in the cavity standing wave pattern, and kept thin enough to avoid the substantial dielectric losses that occur when the sample extends to a region of non-negligible E-field.

The two spherical mirrors of the Fabry-Pérot cavity and the sample are actually placed with their symmetry axes transverse to the magnet bore, and the beam propagating along the bore is coupled into the cavity by a pair of closely spaced diagonal dielectric beam splitters, as shown schematically in *Figure 7*. This scheme was implemented within the constraints of a warm bore diameter of only 45 mm.

Variable coupling into the cavity is achieved interferometrically by moving the dielectric beam splitters relative to each other, while the cavity is tuned to resonance by adjusting the mirror spacing with a rod-driven cam. It was found that the dielectric sheets in the tuning interferometer should be of the same

thickness, with an optimal value of about 0.25mm for 250 GHz. This sheet thickness allowed a wide range of coupling when the spacing between the sheets, d, was varied. Thinner sheets under-coupled the resonator for all values of d, and thicker sheets reduced the resonator Q unnecessarily. The empty cavity finesse was approximately 30, comparable to reported in-line Fabry-Pérot resonators at this frequency (*cf. Table 4*).

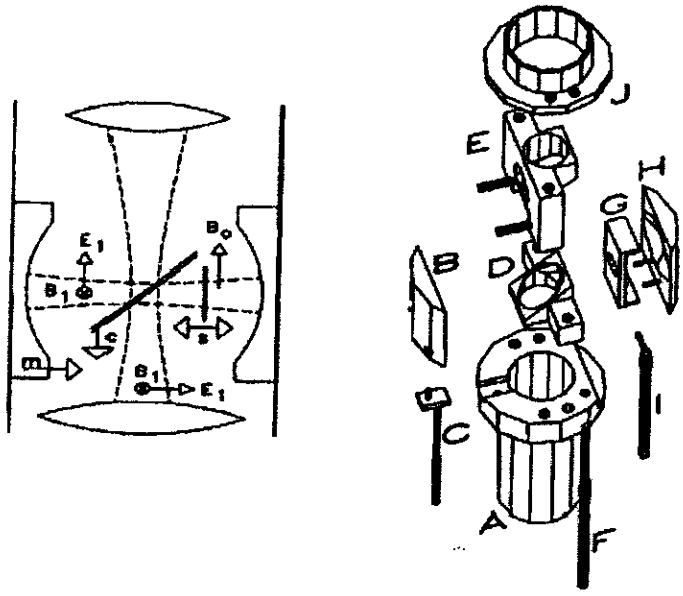

Figure 7. The "shunt" Fabry-Pérot cavity. Left-hand side shows schematic depiction of Gaussian beam in cavity. Right-hand side is drawing of an implementation by Barnes and Freed (Barnes and Freed 1998). (A) and (J) are input and output lens collars, (D) and (E) are coupling window mounts, (B) and (H) are the transverse mirrors, (G) is the sample mount. (C), and (I) are cams to move the mirror spacing and sample placement, respectively, and (F) is a screw to tune the coupling window spacing.

5.5 Whispering Gallery Mode Resonators

The groups at Pisa have developed innovative resonators for high-field EPR known as "Whispering Gallery" mode resonators.(Annino *et al.*, 1999; Annino *et al.*, 1999a; Annino *et al.*, 2000; Annino *et al.*, 2000a) Such resonators consist

of a disc of dielectric material constructed and situated so that the microwave radiation propagates around the outside of the disk. Whispering gallery mode resonators are typically relatively easy to manufacture and have the advantage that they can be scaled to very high frequencies. Thus, many of the impediments to efficient coupling that are encountered in this frequency range for other types of resonators may be circumvented.

Whispering mode galleries can be designed to afford a much higher effective cavity Q than most other types of resonators. One reason for this is that dielectric losses in the resonator material can be much lower than the losses in waveguide- or mirror-based cavities, which are ultimately limited by resistive losses in the conducting materials used to construct them. For configurations in which the sample is placed around the rim of the resonator, filling factors as large $\eta \approx 0.1$ have been reported.(Annino *et al.*, 2000) Thus, in certain optimal cases, the factor $Q\eta$ that determines sensitivity may be much greater than that of the other types of resonators discussed above. It has been suggested that the sensitivity could be optimized for this type of resonator by fabricating the resonator itself from the sample (Annino *et al.*, 2000a) This method could potentially be very sensitive, although limited to samples with a relatively narrow range of dielectric properties.

In fact, the whispering gallery mode resonator is not very useful for samples with appreciable dielectric losses. Because a traveling wave is set up around the rim of the structure at resonance, both magnetic and electric fields penetrate the sample region, so that dielectric losses in the sample can affect the resonator Q quite significantly. A second potentially important limitation of this device is that it is not always feasible to place the sample material around the rim of the resonator.

5.6 Cavities for Crystal rotation

There have been relatively few studies of single crystal rotations at very high EPR fields in comparison with low-field studies. The first report of a cavity designed for crystal rotation at 94 GHz was a waveguide-coupled Fabry-Pérot resonator mounted transversely in the magnet bore (Haindl *et al.*, 1985). This open resonator design has been extensively utilized in the investigation of photosynthetic systems (Burghaus *et al.*, 1992; Hofbauer *et al.*, 2001) because of the relative ease of sample illumination with this design. At 95 GHz, it has also been possible to accomplish single crystal rotation with a TE_{011} cylindrical cavity. (Disselhorst *et al.*, 1995)

At higher frequencies, the relatively small dimensions of cylindrical cavities present some formidable design challenges. One solution to this problem is to use an oversized resonant cavity, as described by Hill *et al.* (1999) for multifrequency single crystal studies in the 30-120 GHz range. At the very highest frequencies, however, the only practicable accommodation for crystal rotation seems to be a Fabry-Pérot resonator. Earle and Freed (1999), have

given a detailed description of a single-axis goniometer designed for operation with a Fabry-Pérot resonator at 250 GHz, shown schematically in *Figure 8*. The device was implemented with a warm bore diameter of 45 mm.

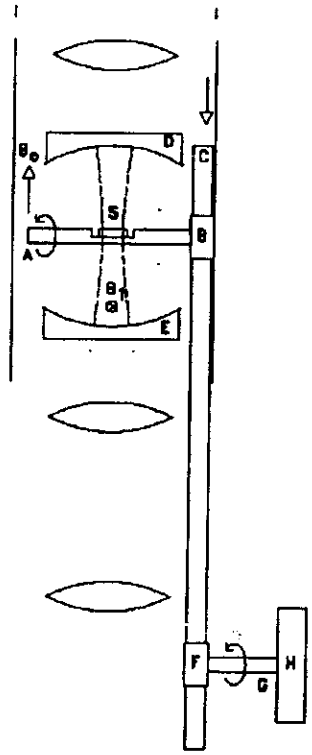

Figure 8. Single-crystal rotation within a Fabry-Pérot cavity. A: sample rod, B: pinion, C: rack, D: upper spherical mirror, E: bottom spherical mirror, F: pinion, G: vacuum feed through control rod, H: vernier dial.

The orientation of the spectrometer field B_0 in this figure is along the axis of the resonator, and that of the linearly polarized B_1 field is perpendicular to the resonator axis. Sample rotation is accomplished via a support rod fabricated from Rexolite (cross linked polystyrene). The orientation of the support rod is perpendicular to the B_0 field, but it may be varied with respect to the B_1 field direction. This feature allows optimization of the rotation axis with respect to the B_1 direction in cases where the transition probability may be orientation-

dependent, as in transition metals. Rotation is accomplished by a rack and pinion drive that is always operated in the direction indicated by the arrow in *Figure 8*. The drive is lubricated with molybdenum disulfide or Apiezon 'T' grease at room temperature, and graphite at low temperature. Space constraints limit the travel of the rack to approximately 300° degrees of rotation, which is ample for collecting rotation data in one plane. A knife-edge vernier scale allows the rotation setting to be read to at least ±0.3°. The significant scattering from support rod does reduce the transmitted power in comparison with simple transmission Fabry-Pérot designs; however, the reported finesse of ≈40 is quite comparable. Double O-ring seals for the actuator shaft, mirror, and support assembly permit evacuation of the apparatus, and the housing of the cavity and goniometer was fabricated from G-10 resin (garolite) to minimize heat conduction for use of the goniometer at or below 77K. This resonator has been applied to single-crystal studies of transition metal ions in inorganic crystals such as Ni doped $CdCl_6$ at temperatures down to about 250 K. (Misra *et al.*, 2001)

6. FIELD MODULATION

Magnetic field modulation is a serious technical issue for high field cw EPR. The main problem is the increased Lorentz forces on the modulation coils resulting from coupling to the much larger spectrometer fields employed. Direct mechanical contact between the modulation coils and the cavity components (or sample) has caused significant problems in a number of systems, presumably because of the large forces involved and the high sensitivity of the cavity to very small dimensional changes. It is therefore advantageous to isolate the modulation coils physically from the resonator when the bore diameter is large enough to permit such a separation.

A second significant problem with a number of different cavity configurations is eddy current heating resulting from the high field modulation amplitudes that are often required for the broad lines that can occur at high EPR frequencies. As is the case at lower frequencies, this effect can be minimized by fabricating the cavity walls or resonator mirrors with the minimum amount of metal possible. One strategy that has been successfully employed for spherical Fabry-Pérot cavity mirrors has been to flash a layer of chromium (for improved adhesion) onto a plano-concave spherical lens with the appropriate radius of curvature and then sputter a thick layer of noble metal (several skin depths for high reflectivity) on top of the chromium flash to define a diffraction-limited reflecting mirror.

At high fields, one does have greater flexibility in the choice of modulation frequency than at X-band. The 100 kHz commonly employed at X-band corresponds to the frequency at which the $1/f$ noise associated with mixers starts

to become negligible. The InSb mixers or Schottky heterodyne systems more commonly used at higher EPR frequencies do not have this constraint, and modulation frequency may be advantageously reduced as low as 1 kHz, although microphonic signals can be significant at such low frequencies. For very broad lines, where the amplitude of the magnetic field modulation may be only a small fraction of the line width, there are some advantages to dispensing with magnetic field modulation altogether in such cases and using alternative methods for signal processing.

7. A MATRIX METHOD FOR LOSSY SAMPLES

A major challenge in applying high-field EPR to biological samples near physiological temperatures has been its lack of sensitivity for aqueous samples due to the significant dielectric losses of water at millimetre-wave frequencies. Although the dielectric loss tangent of water generally decreases with frequency above 20 GHz, it is still necessary to avoid overlap of the sample volume with the E field in the resonator. Thus, the lower sample volume required at smaller λ tends to reduce the gain in sensitivity that would otherwise result from lower dielectric losses.

As noted in Section 2.2.2, open resonators offer some geometric advantages for minimizing E-field overlap with the maximum possible sample volume. In simplest terms, this derives from the fact that the E-field nodes are planar or nearly so in such resonators. Therefore, despite the much lower FOM typically obtained for Fabry-Pérot cavities, they become competitive for very thin, lossy samples. It has proved possible to design sample cells for a Fabry-Pérot transmission cavity that afforded an absolute sensitivity of 10^8 spins Gauss^{-1} under favorable conditions,(Earle and Freed 1999) which is adequate for studies of many aqueous samples of biological interest. In their initial demonstration of a cavity design for aqueous samples, Barnes and Freed 1997 described a cell consisting of a thin layer of water sandwiched between two dielectric windows mounted transversely in a FPI. A similar sample cell has been utilized at 220 GHz by Cardin *et al.*, 1999.

Spectrometer sensitivity depends strongly upon the sample geometry in aqueous samples, and especially upon the thickness of the aqueous layer and surrounding windows. Barnes and Freed carried out an analysis based on transmission line reflection coefficients to calculate sensitivity for different cavity geometries, but did not give details of this method. Earle *et al.* (2001) have recently described a similar transfer matrix method that can be applied to a wide variety of cavity design problems involving samples with high dielectric loss (including solvents other than water) and different dielectric materials. We present a summary of the method here and demonstrate some simple applications.

7.1 Basic Transfer Matrix Method

The transfer matrix method was originally developed for analyzing transmission lines.(Collin, 1992; Budil *et al.*, 2000) Its applicability to cavity design derives from the fact that individual Gaussian modes propagating through space are reasonably well represented as waves on a transmission line.(Born and Wolf, 1980) For this approximation to apply, the sample should be placed as close as possible to the beam waist in the cavity, where the beam divergence is slow and the phase front is essentially planar. Similarly, beam growth outside of the sample region may be neglected with the use of one or two spherical mirrors that are correctly matched to the phase front curvature of the beam. Given that most Fabry-Pérot resonators are operated in a regime where the phase front at the location of the curved mirror is in the near field of the beam waist, *i.e.*, where the beam divergence is limited, transmission line methods offer a useful approximation to a more rigorous analysis including corrections for beam growth within the sample and cavity.

An optical element is represented by a two-by-two matrix **M**, which relates the input and output *E*-fields and *B*-fields of the element as follows:

$$\begin{pmatrix} E_{out} \\ B_{out} \end{pmatrix} = \mathbf{M}\begin{pmatrix} E_{in} \\ B_{in} \end{pmatrix} = \begin{pmatrix} \mathcal{A} & \mathcal{B} \\ C & \mathcal{D} \end{pmatrix}\begin{pmatrix} E_{in} \\ B_{in} \end{pmatrix} \qquad [24]$$

A useful property of this representation is that the output fields for a given element are the input fields of the next element. Thus, a series of elements may be represented by the product of the matrices for each element. The $\mathcal{A}$, $\mathcal{B}$, C, and $\mathcal{D}$ elements of a system matrix $\mathbf{M}_{sys}$ are then used to calculate the field transmission and reflection coefficients of the system as follows (Goldsmith 1998):

$$r = \frac{E_r}{E_i} = \frac{\mathcal{A}Z_{out} + \mathcal{B} - CZ_{in}Z_{out} - \mathcal{D}Z_{in}}{\mathcal{A}Z_{out} + \mathcal{B} + CZ_{in}Z_{out} + \mathcal{D}Z_{in}}$$
$$t = \frac{E_t}{E_i} = \frac{2Z_{out}}{\mathcal{A}Z_{out} + \mathcal{B} + CZ_{in}Z_{out} + \mathcal{D}Z_{in}} \qquad [25]$$

where E_i, E_r, and E_t are respectively the amplitudes of the incident, reflected, and transmitted fields, and Z_{in} and Z_{out} are the input and output impedances, which are generally the impedance of free space, $Z_0 = \sqrt{\mu_0/\varepsilon_v} = 377\ \Omega$. The field coefficients r and t are in general complex-valued; the power transmission, reflection, and absorption coefficients may be calculated from these as follows: $\mathcal{T}=|t|^2$, $\mathcal{R}=|r|^2$, and $\mathcal{A}=1-(\mathcal{T}+\mathcal{R})$.

A wide variety of open-resonator configurations may be reproduced using only two basic matrices: the first matrix represents a mirror, and the second, a dielectric slab, which may be applied to dielectric windows, an EPR sample with or without dielectric losses, or transmission through free space.

The mirror matrix is simply the matrix for a shunt impedance Z_m across a transmission line, with the explicit form (Montgomery *et al.*, 1948; Harvey, 1963; Ulrich, 1967; Goldsmith, 1982; Lesurf, 1990; Budil *et al.*, 2000)

$$\mathbf{M}_m(Z_m) = \begin{pmatrix} 1 & 0 \\ 1/Z_m & 1 \end{pmatrix} \qquad [26]$$

The effective mirror impedance Z_m is typically small, (Born and Wolf, 1980) and is purely reactive (i.e., $Z_m = iX_m$) for perfect (i.e., loss-free) mirror. Complex-valued impedance can be used to account for radiation losses, mode conversion, and diffraction from an aperture or resistive losses in the mirror metal.

The general form for a matrix $\mathbf{M}_d$ representing a dielectric layer is

$$\mathbf{M}_d(\varepsilon,\mu,d) = \begin{pmatrix} \cosh ik_0 d\sqrt{\mu\varepsilon} & \sqrt{\dfrac{\mu}{\varepsilon}}\sinh ik_0 d\sqrt{\mu\varepsilon} \\ \sqrt{\dfrac{\varepsilon}{\mu}}\sinh ik_0 d\sqrt{\mu\varepsilon} & \cosh ik_0 d\sqrt{\mu\varepsilon} \end{pmatrix} \qquad [27]$$

in which $k_0 = 2\pi/\lambda_0$ is the wave number of the radiation in free space, d is the path length through the material, $\varepsilon = \varepsilon_v(1 + \chi_e)$, where χ_e is the electric susceptibility of the medium and ε_v is the vacuum permittivity, equal to 8.85×10^{-12} F m^{-1}. For propagation through free space, $\varepsilon = \varepsilon_v$, and $\mu = \mu_0$, the vacuum permeability, which has a value of $4\pi\times10^{-7}$ H m^{-1}. Materials with dielectric loss are represented by a complex-valued permittivity. In the presence of an EPR-active sample, $\mu = \mu_0(1+\chi)$, where χ is the EPR sample susceptibility.

The general approach is to multiply the transfer matrix representations for a given configuration of the different cell components. One then uses the resulting system matrix to determine transmission and reflection coefficients T and R. Finally, sensitivity to EPR absorption or dispersion is obtained by taking the partial derivatives of T or R with respect to the components χ' and χ'' of the magnetic susceptibility, typically using a numerical forward-differences approximation. For example, to determine the EPR sensitivity in transmission mode, T would be calculated for the system matrix according to the second of Eqs. [25] assuming $\chi=0$ for the matrix representing the sample. It is then

recalculated setting χ' or χ'' set to some small number δ (typically about 10^{-6}) and the sensitivity approximated as $\Delta T/\delta$.

Careful optimization of windows and sample dimensions depends critically on accurate knowledge of ε at far-infrared frequencies for the mirrors and window materials as well as for the sample itself. For dielectric windows, Goldsmith 1998, has tabulated ε' and ε'' for a variety of useful materials. Extensive measurements of ε have also been made for water as a function of frequency and temperature.(Afsar and Hasted, 1977; Hasted *et al.*, 1985; Hasted *et al.*, 1987; Barthel *et al.*, 1990) These results show that both ε' and ε'' decrease with frequency above 20 GHz, but exhibit resonant absorption bands due to intermolecular librations near 10 THz (Hasted, 1973).

For most accurate work, it may also be necessary to consider the solute in the sample. High-frequency dielectric relaxation spectroscopy has suggested that ε is significantly altered at mm-wave frequencies by electrolytes and hydrogen-bonding solutes such as sucrose or glycerol, which are often added to biological samples to modify the effective viscosity or to promote glass formation.(Wei and Sridhar, 1990) Indeed, there is some evidence from dielectric studies that macromolecules themselves modify the effective ε at very high frequencies.(Wei *et al.*, 1994)

Tabulations of complex permittivity for other solvents of interest are generally not available in the 150 GHz to 1 THz frequency range. One may often estimate ε using a modified Debye form for solvent dipole relaxation:

$$\varepsilon = \varepsilon_\infty + \frac{\varepsilon_0 - \varepsilon_\infty}{1 + i\omega\tau} - \frac{i\sigma_0}{\omega\varepsilon_v} \qquad [28]$$

where ω is the angular frequency at which ε is to be calculated, ε_0 is the static permittivity, ε_∞ is the limiting permittivity at infinite frequency, τ is the rotational correlation time of the solvent, and σ_0 is the DC conductivity of the sample, and ε_v is the permittivity of vacuum defined above. These parameters have been tabulated for a wide variety of solvents and temperatures (Buckley and Maryott, 1958); A short compilation of Debye parameters for a small selection of relevant solvents for EPR is given in *Table 5*.

7.2 Application to Cavity Tuning

The formalism described above will now be illustrated for a basic open resonator configuration similar to that utilized by Barnes and Freed. The cell, which is depicted in *Figure 9* consists of an aqueous layer of thickness d containing the EPR sample with a quartz windows of thickness d_w on either side. The cell is placed between the mirrors at distances d_1 and d_2 from them.

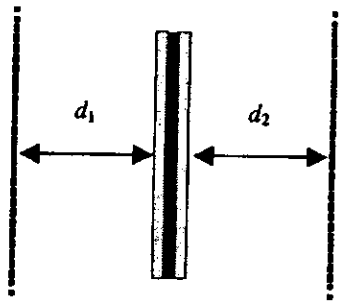

Figure 9. Schematic diagram of aqueous sample arrangement in a Fabry-Pérot resonator. The sample is placed between two dielectric windows located at distances d_1 and d_2 from the partially reflective mirrors of the resonator (dotted lines)

A typical impedance for a practically realizable partially reflective mirror with some resistive losses is $Z_m = Z_0(0.2–4i)$ corresponding to a power reflectivity of about 97%. Using this value together with permittivity of $\varepsilon_d = 4.54$ for fused quartz and $\varepsilon_s = 5.5–6.0i$ for water at 250 GHz, we may form a matrix product for the configuration shown in *Figure* 9 as follows:

$$\begin{aligned}\mathbf{M}_{\text{system}} = {} & \mathbf{M}_m(Z_m)\cdot\mathbf{M}_d(1,1,d_1)\cdot\mathbf{M}_d(\varepsilon_d,1,d_d)\cdot\mathbf{M}_d(\varepsilon_s,\mu_s,d_s) \\ & \times\mathbf{M}_d(\varepsilon_d,1,d_d)\cdot\mathbf{M}_d(1,1,d_2)\cdot\mathbf{M}_m(Z_m)\end{aligned} \quad [29]$$

where d_d and d_s respectively represent the thickness of the dielectric window and the sample, and d_1 and d_2 are the mirror spacings defined in *Figure 9*.

The power transmission coefficient $\mathcal{T}$ is calculated by applying Eqs. [25] to the matrix product and it plotted as a function of d_1 and d_2 in *Figure 10*. The peaks observed in the plot correspond to the power transmission maxima that occur when the effective path length through the cavity (including windows and sample) is near a half-integral number of wavelengths. A plot of reflected power would exhibit a series of troughs corresponding to the peaks in *Figure 10*.

The power maxima in the d_1, d_2 space are typically quite elongated, with the approximate long axis of the peak lying parallel to the line d_1+d_2 = constant. This feature suggests an optimal approach for tuning Fabry-Pérot cavities. Motion of either mirror along lines (a) and (a′) will in general produce a series of peaks spaced at $\lambda/2$, and this qualitative pattern can be observed with the motion of one mirror over a wide range of fixed positions for the other mirror, even far away from the transmission maximum.

To move towards the maximum of the peak from arbitrary mirror positions requires alternating one-mirror adjustments, resulting in a time-consuming and tedious zigzag approach to the optimal position. It is much more efficient to make adjustments along the major axes of the transmission peak: specifically

along the directions of constant d_1+d_2 and constant d_1-d_2. In other words, the fastest procedure is to adjust the mirror spacing with a jaw-like symmetric motion of the two mirrors, parallel to line (b) in *Figure 10*, and then move the sample location relative to the two mirrors, corresponding to adjustment along line (c).

Table 5. Dielectric parameters for a selection of solvents

Formula	T/°C	$\varepsilon_0/\varepsilon_r$	$\varepsilon_\infty/\varepsilon_r$	τ/ps
H_2O	0.0	88.20	5.00	17.7
	10.0	84.00	5.00	16.6
	20.0	80.40	5.20	12.3
	30.0	76.50	5.20	9.3
H_2SO_4	20.0	110.00	5.00	478
CS_2	20.0	2.64	2.65	4.5
$CHCl_3$	25.0	4.72	2.09	7.4
CH_3OH	-109.9	82.17	9.80	812
	30.0	31.65	5.50	42.5
C_2H_5OH	−142.6	79	8	2.65×10^6
	30	23.56	4.2	113
$C_2H_2(OH)_2$	25	41.3	5.4	112
C_3H_6O	20	21.2	1.9	3.3
C_3H_6OH	−95.7	47.1	4	1.02×10^6
	20	19	3.2	920
$C_3H_5(OH)_3$	−74.6	76.2	4.18	9.61×10^{11}
	20	34.1	4.8	1.80×10^3
$C_4H_{10}O$	4	4.7	0	2.81
C_6H_{14}	20	1.89	0	7.43
$C_6H_{10}O$	1	17.01	2.21	14.4
C_7H_8	20	2.391	0	7.43
$C_6H_5NH_2$	20	6.89	0.028	19.6
C_4H_4O	20	2.954	0	2.18

7.3 Signal Phase Effects

The transfer matrix method also gives some insights into some of the significant effects that a Fabry-Pérot cavity may have on the EPR signal phase (that is, the admixture of absorption and dispersion). It has not been widely acknowledged in the literature that the observed phase is quite sensitive to both the mirror spacing and the sample position in the Fabry-Pérot. *Figure 11* shows

the calculated EPR sensitivity to both absorption and dispersion for both transmission and reflection cavities. For reference, the transmitted or reflected power is also plotted. At the center of the transmission or reflection peak the sensitivity to the dispersion signal is zero, and one observes a pure absorption signal. However, small displacements of either the sample or the mirrors from their optimal positions can both increase the sensitivity to the dispersion signal and decrease sensitivity to the absorption signal, leading to an effective phase shift in the observed EPR signal.

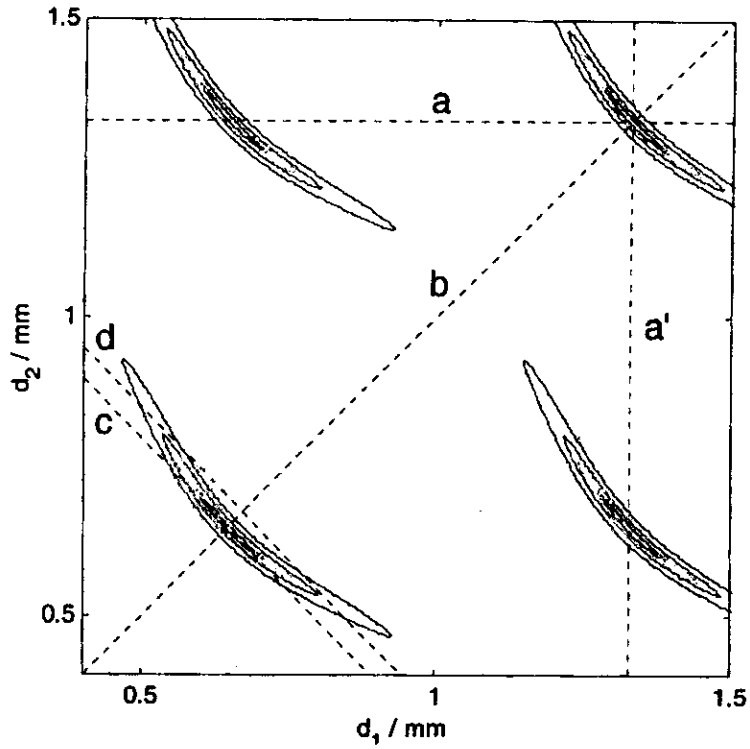

Figure 10. Power transmission coefficient for the cavity shown in Figure 1 as a function of mirror spacings d_1 and d_2. Dotted lines correspond to various types of cavity mirror motion: (a) motion of one mirror with the other one fixed, (b) symmetric motion of the mirrors about the sample, (c) and (d) motion of the mirrors in the same direction, equivalent to motion of the sample relative to fixed mirrors.

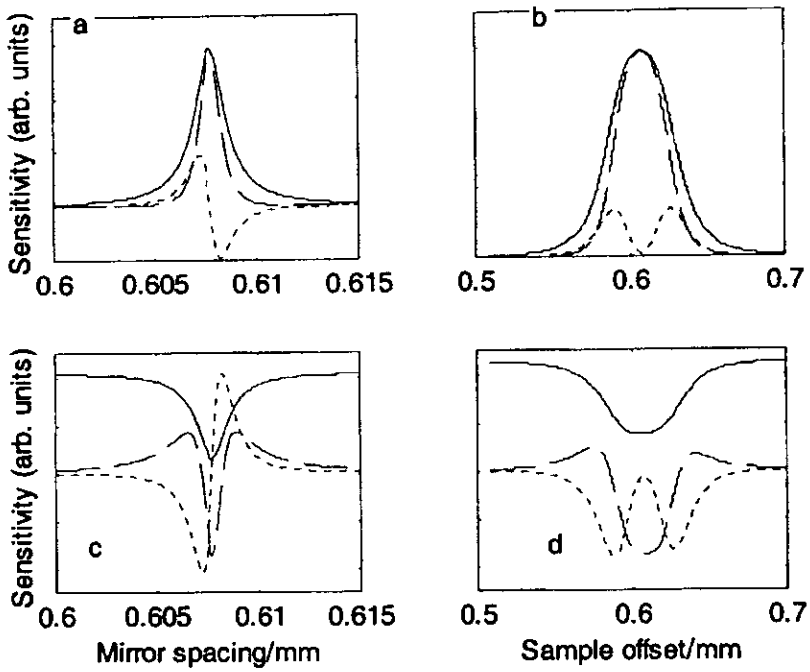

Figure 11. Millimeter wave power (solid lines) and EPR sensitivity to absorption (dashed lines) and dispersion (dotted lines) for mirror displacements (left-hand side) and sample displacements (right-hand side) for transmission mode (top: a and b) and reflection mode (bottom: c and d).

7.4 Solvent Effects

The original application of the transmission line analysis carried out by Barnes and Freed 1997, was to find the optimal sample thickness for an aqueous sample at 250 GHz. *Figure 12a* demonstrates this type of optimization for solvents with different dielectric properties using quartz windows with a fixed thickness of 0.17 mm. Sensitivity to absorption χ'' was calculated as a function of sample thickness for water, methanol, ethanol, and toluene in order to illustrate cavity behavior for both polar and non-polar solvents. For each curve, the mirror spacing was adjusted to maximize sensitivity for each sample thickness using a one-dimensional search algorithm (Press *et al.*, 1992).

The curves in *Figure 12a* can be qualitatively understood as follows. For the thinnest samples, the sensitivity is limited by the number of spins and thus increases linearly with sample thickness regardless of the sample's dielectric

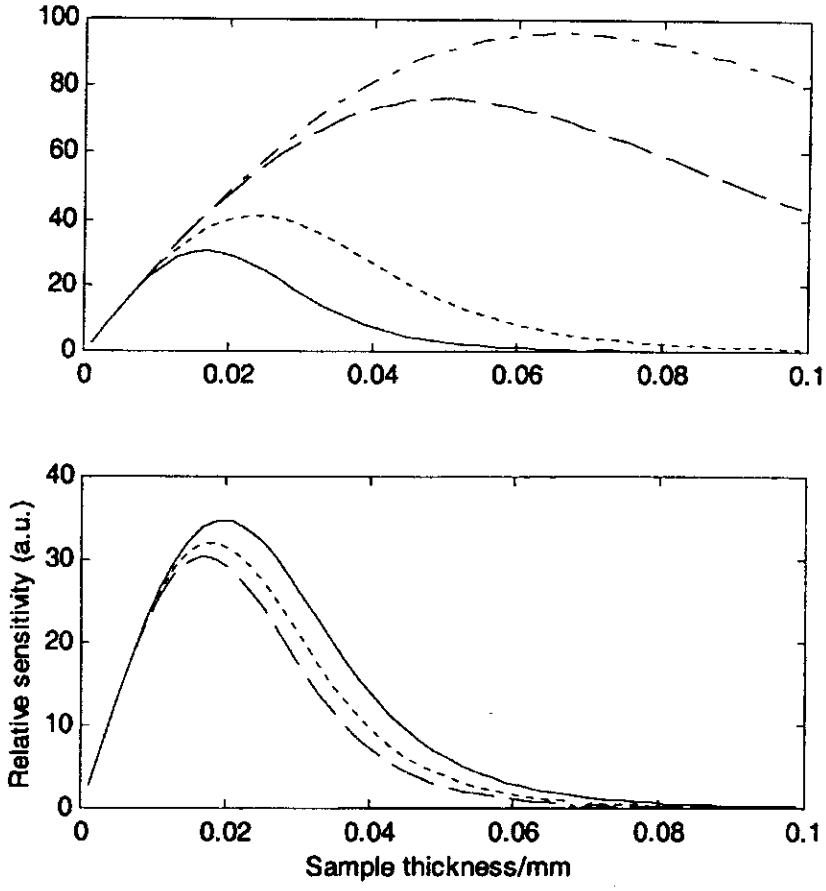

Figure 12. EPR sensitivity as a function of sample thickness for various solvents using a fixed window thickness of 0.17 mm. (a) Sensitivity curves for solvents of different polarity: water (—), methanol (---), ethanol (— —), and toluene (— · —). (b) Sensitivity curves for water at different temperatures: 20°C (—), 10°C(---), and 0°C (— —). Calculated using parameters given in Tables 1 and 2.

losses. However, since these losses depend exponentially upon the beam path length they become dominant as the sample thickness increases. Thus, lossy samples exhibit a maximum at smaller thickness, whereas the linear

increase in sensitivity extends to longer path lengths in low-loss solvents such as toluene, leading to a maximum at larger sample thickness
and substantially greater concentration sensitivity. One somewhat surprising result from the analysis of Earle *et al.* (2001) is the significant effect of temperature on sensitivity for aqueous samples.
Figure 12b shows EPR sensitivity as a function of sample thickness for an aqueous sample at three different temperatures. When the sample is slightly thicker than the optimum value, the sensitivity can decrease by as much as a factor of two upon going from room temperature to 0°. Although this neglects changes in sample volume with temperature, which would likely compensate for the sensitivity loss to some degree, this plot illustrates the critical dependence of EPR sensitivity on sample dielectric properties. Such considerations are important for temperature-dependent studies in biological samples, where it is also frequently necessary to freeze a sample in order to obtain magnetic parameters from the rigid limit spectrum.

Figure 12b also shows that the sensitivity is relatively unaffected for samples slightly thinner than the optimum value, suggesting that this is a better choice for the sample thickness when temperature-dependent studies are to be performed in aqueous systems.

We conclude by demonstrating how to calculate quantities such as Q factors and coupling parameters for different Fabry-Pérot configurations. These quantities depend upon the effective input impedance of the cavity contents, i.e. the free space-window-sample-window-free space elements between the mirrors, when it is terminated with output impedance Z_{out}. The effective impedance can be obtained from the system matrix for the cavity as follows:

$$Z_{in} = \frac{\mathcal{A}Z_{out} + \mathcal{B}}{\mathcal{C}Z_{out} + \mathcal{D}} \qquad [30]$$

The impedance "seen" by the input mirror (an arrangement suitable for a reflection mode resonator) is then the effective impedance of the cavity contents when terminated by a perfectly reflecting short ($Z_{out} = 0$):

$$Z_{eff} = \frac{\mathcal{B}}{\mathcal{D}} \qquad [31]$$

The unloaded cavity quality factor Q_U can be estimated directly from Z_{eff}:

$$Q_U = \frac{\mathrm{Im}\{Z_{eff}\}}{\mathrm{Re}\{Z_{eff}\}} \qquad [32]$$

and the coupling parameter β for the mirror obtained from the mirror impedance and effective cavity impedance as follows: (Montgomery *et al.*, 1948)

$$\beta = \frac{|X_m|^2}{Z_0 \, \mathrm{Re}\{Z_{eff}\}} \qquad [33]$$

These quantities can then be used to calculate the loaded quality factor of the cavity, Q_L for comparison with experimental measurement according to Eqs. [12] For a reflection cavity β_2 is taken to be zero. Thus, the transfer matrix formalism can be used to calculate quantities that allow direct comparison with other types of sample cavity.

For a transmission cavity, the coupling parameters will be different if the mirror reflectivity differ, or if the cavity elements are disposed asymmetrically within the cavity. In order to apply the transfer matrix formalism to the transmission mode case, one should replace the short ($Z_{out} = 0$ in Eq. [30]) with a second shunt reactance in parallel with the characteristic impedance of the output transmission line, Z_0.

8. CONCLUSION

In this chapter, we have presented a comparison of various resonant and non-resonant structures that may be used to optimize the sensitivity of HF EPR under various experimental conditions. One of the main points of this review is that there is no universal sample holder that is the best choice for all applications. Nevertheless, some general guidelines may be formulated. Very high-Q resonators analogous to the cavities used in waveguide-based systems have afforded the highest achievable sensitivity to date, and development of such devices is still active, especially at the highest frequencies. However, a number of applications, particularly for biological samples, impose additional requirements that cannot easily be satisfied by designs based on fundamental mode cavities. Examples include membrane samples, aqueous samples, samples requiring illumination such as photosynthetic systems, and crystals. For these applications, the Fabry-Pérot cavity offers much greater flexibility at some cost in sensitivity if one is limited to conventional designs. The development of reduced dimension Fabry-Pérot resonators may address some of the shortcomings of conventional designs and this will be a major area of future development in our view. In the end, careful experimental design, including accurate evaluation of absolute versus concentration sensitivity, sample losses and sample size will all inform the optimum choice of resonant or non-resonant structure with which to do HF EPR spectroscopy.

A number of analytical tools that can facilitate the experimental design process were presented in the hope that they may be of use to the HF EPR community and perhaps aid the design and development of subsequent generations of HF EPR spectrometers with even higher sensitivity than currently available.

Although this review has concentrated on structures appropriate for CW work, where appropriate, considerations that are relevant for pulse work have been included as well. Spectral coverage is the main issue for any but the simplest of pulsed experiments in HF ESR and these promises to be a major area of research in the future.

ACKNOWLEDGEMENT. The authors are grateful to Prof. Graham M. Smith for his contributions to the discussion of cavity sensitivity. Support from NSF awards MCB 9600940 (DEB) and CHE 9615910 and NIH grant RR07126-07 (KAE) is gratefully acknowledged. The Cornell Theory Center is acknowledged for the use of their facilities in performing some of the calculations reported here.

REFERENCES

Afsar, M.N. and Hasted, J.B., 1977. Measurement of the optical constants of liquid water and water-d2 between 6 and 450 cm-1. *J. Opt. Soc. Am.* **67**: 902-904.

Annino, G., Bertolini, D., *et al.* 2000. Dielectric properties of materials using whispering gallery dielectric resonators: Experiments and perspectives of ultra-wideband characterization. *J. Chem. Phys.* **112**: 2308-2314.

Annino, G., Cassettari, M., *et al.* 2000a. Whispering gallery mode dielectric resonators in EMR spectroscopy above 150 GHz: problems and perspectives. *Applied Magnetic Resonance* **19**: 495-506.

Annino, G., Cassettari, M., Longo, I. and Martinelli, M. 1999. Dielectric Resonators in ESR: Overview, Comments and Perspectives. *Appl. Magn. Reson.* **16**.

Annino, G., Cassettari, M., *et al.* 1999a. A novel probe head for high-field, high-frequency electron paramagnetic resonance. *Rev. Sci. Instrum.* **70**: 1787-1793.

Barnes, J.P. and Freed, J.H. 1997. Aqueous sample holders for high-frequency electron spin resonance. *Rev. Sci. Instrum.* **68**: 2838-2846.

Barnes, J.P. and Freed, J.H. 1998. A "shunt" Fabry-Perot resonator for high-frequency electron spin resonance utilizing a variable coupling scheme. *Rev. Sci. Instrum.* **69**: 3022-3027.

Barthel, J., Bachhuber, K., Buchner, R. and Hetzenauer, H. 1990. Dielectric spectra of some common solvents in the microwave region. Water and lower alcohols. *Chem. Phys. Lett.* **165**: 369-73.

Becerra, L., Gerfen, G., *et al.* 1995. A spectrometer for dynamic nuclear polarization and electron paramagnetic resonance at high frequencies. *J. Magn. Reson. Ser. A* **117**: 28-40.

Born, M. and Wolf, E. 1980. *Optics*. Oxford, Permagon Press.

Brezgunov, A.Y., Dubinskii, A.A., *et al.* 1991. Pulsed EPR in 2-mm band. *Appl. Magn. Reson.* **2**: 715-28.

Buckley, F. and Maryott, A.A. 1958. Tables of dielectric dispersion data for pure liquids and dilute solutions. Washington, D.C., National Bureau of Standards: 96.

Budil, D.E., Ding, Z., Smith, G.R. and Earle, K.A. 2000. Jones Matrix Formalism for Quasioptical EPR. *J. Magn. Reson.* **144**: 20-34.

Budil, D.E., Earle, K.A. and Freed, J.H. 1993. Full determination of the rotational diffusion tensor by electron paramagnetic resonance at 250 GHz. *J. Phys. Chem.* **97**: 1294-303.

Budil, D.E., Earle, K.A., Lynch, W.B. and Freed, J.H. 1989. Electron paramagnetic resonance at 1 millimeter wavelengths. in *Advanced EPR: Applications in biology and biochemistry*. A. J. Hoff. Amsterdam, Elsevier: 307-340.

Burghaus, O., Rohrer, M., *et al.* 1992. A novel high-field/high-frequency EPR and ENDOR spectrometer operating at 3 mm wavelength. *Meas. Sci. Technol.* **3**: 765-774.

Burghaus, O., Toth-Kischkat, A., Klette, R. and Moebius, K. 1988. Proton ENDOR at a microwave frequency of 97 GHz. *J. Magn. Reson.* **80**: 383-8.

Cardin, J.T., Kolaczkowski, S.V., Anderson, J.R. and Budil, D.E. 1999. Quasioptical design for an EPR spectrometer based on a horizontal-bore superconducting solenoid. *Appl. Magn. Reson.* **16**: 273-292.

Clarke, R.N. and Rosenberg, C.B. 1982. Fabry-Perot and open resonators at microwave and millimetre wave frequencies, 2-300 GHz. *J. Phys.E. Sci. Instrum.* **15**: 9-24.

Collin, R.E. (1992). *Foundations for Microwave Engineering*. New York,, McGraw-Hill, Inc.

Disselhorst, J.A.J.M. and Schmidt, J. 2000. Cylindrical cavity for EPR spectroscopy at 360 GHz. *START Meeting on High-Field EPR Techniques and Applications*, Amsterdam.

Disselhorst, J.A.J.M., van der Meer, H., Poluektov, O.G. and Schmidt, J. 1995. A pulsed EPR and ENDOR spectrometer operating at 95 GHz. *Journal of Magnetic Resonance, Series A* **115**: 1064-1858.

Doane, J. 1985. Propagation and mode coupling in corrugated and smooth-wall circular waveguides. in *Infrared and Millimeter Waves*. K. J. Button. New York, Wiley. **13**: 123-170.

Doubinski, A.A. 1998. Advanced EPR in millimeter bands and very high fields. *Electron Paramagnetic Resonance* **16**: 211-233.

Earle, K.A., Budil, D.E. and Freed, J.H. 1996a. Millimeter wave electron resonance using quasioptical techniques. *Adv. Magn. Opt. Reson.* **19**: 253-323.

Earle, K.A., Tipikin, D.S. and Freed, J.H. 1996b. Far-infrared electron-paramagnetic-resonance spectrometer utilizing a quasioptical reflection bridge. *Rev. Sci. Instrum.* **67**: 2502-2513.

Earle, K.A. and Freed, J.H. 1999. Quasioptical hardware for a flexible FIR-EPR spectrometer. *Appl. Magn. Reson.* **16**: 247-272.

Earle, K.A., Zeng, R. and Budil, D.E. 2001. Transfer Matrix Method for Optimizing Quasioptical EPR Cavities. *Appl. Magn. Reson.* **21**: 275-287.

Eaton, G.R. and Eaton, S.S. 1999. High-field and high-frequency EPR. *Appl. Magn. Reson.* **16**: 161-166.

Fuchs, M.R., Prisner, T.F. and Mobius, K. 1999. A high-field/high-frequency heterodyne induction-mode electron paramagnetic resonance spectrometer operating at 360 GHz. *Rev. Sci. Instrum.* **70**: 3681-3683.

Goldsmith, P.F. 1982. Quasi-optical techniques at millimeter and submillimeter wavelengths. in *Infrared and Millimeter Waves*. K. J. Button. New York, Academic Press. **6**: 277-344.

Goldsmith, P.F. 1998. *Quasioptical Systems*. Piscataway, NJ, IEEE Press/Chapman & Hall Publishers.

Goy, P. 1983. Millimeter and Submillimeter Waves Interacting With Giant Atoms (Rydberg States). in *Infrared and Millimeter Waves*. K. J. Button. New York, Academic Press. **8:** 352--386.

Grinberg, O.Y., Dubinskii, A.A. and Lebedev, Y.S. 1983. Electron paramagnetic resonance of free radicals in the two-millimeter wavelength range. *Usp. Khim.* **52:** 1490-513.

Haindl, E., Moebius, K. and Oloff, H. 1985. A 94 GHz EPR spectrometer with Fabry-Perot resonator. *Z. Naturforsch., A: Phys., Phys. Chem., Kosmophys.* **40A:** 169-72.

Harvey, A.F. (1963). *Microwave Engineering*. New York, Academic Press.

Hassan, A.K., Maniero, A.L., *et al.* 1999. High-Field EMR: Recent CW Developments at 25 Tesla, and Next-Millennium Challenges. *Appl. Magn. Reson.* **16**: 299-308.

Hassan, A.K., Pardi, L.A., *et al.* 2000. Ultrawide Band Multifrequency High-Field EMR Technique: A Methodology for Increasing Spectroscopic Information. *J. Magn. Reson.* **142**: 300-312.

Hasted, J.B. (1973). *Aqueous Dielectrics*. London, Chapman and Hall.

Hasted, J.B., Husain, S.K., Frescura, F.A.M. and Birch, J.R. 1985. Far-infrared absorption in liquid water. *Chem. Phys. Lett.* **118**: 622-5.

Hasted, J.B., Husain, S.K., Frescura, F.A.M. and Birch, J.R. 1987. The temperature variation of the near millimeter wavelength optical constants of water. *Infrared Phys.* **27**: 11-15.

Hill, S., Dalal, N.S. and Brooks, J.S. 1999. A multifrequency-resonator-based system for high-sensitivity high-field EPR investigations of small single crystals. *Applied Magnetic Resonance* **16**: 237-245.

Hofbauer, W., Zouni, A., *et al.* 2001. Photosystem II single crystals studied by EPR spectroscopy at 94 GHz: the tyrosine radical YD×. *Proceedings of the National Academy of Sciences (USA)* **98**: 6623-6628.

Jones, E.M.T. and Cohn, S.B. 1955. Surface matching of dielectric lenses. *J. Appl. Phys.* **26**: 452-7.

Krzystek, J., Pardi, L., Hassan, A. and Brunel, L.C. 1996. Millimeter and submillimeter wave Electron Paramagnetic Resonance spectroscopy. *Proc. SPIE-Int. Soc. Opt. Eng.* **2842**: 255-262.

Lesurf, J.C.G. 1990. *Millimetre-wave Optics, Devices, and Systems*. Bristol, Adam Hilger.

Lynch, W.B., Earle, K.A. and Freed, J.H. 1988. A 1-mm wave ESR spectrometer. *Rev. Sci. Instrum.* **59**: 1345-51.

Marcuvitz, N. (1951). *Waveguide Handbook*. New York, McGraw-Hill.

Matsui, T., Araki, K. and Kiyokawa, M. 1993. Gaussian-Beam Open Resonator with Highly Reflective Circular Coupling Regions. *IEEE Trans. Microwave Theory Tech.* **MTT-41**: 1710-1714.

Misra, S.K., Andronenko, S.I., Earle, K.A. and Freed, J.H. 2001. Single-crystal EPR studies of transition-metal ions in inorganic crystals at very high frequency. *Applied Magnetic Resonance* **21**: 549-561.

Möbius, K. 2000. Primary processes in photosynthesis: what do we learn from high-field EPR spectroscopy? *Chem. Soc. Rev.* **29**: 129-139.

Moll, H.P., Kutter, C., *et al.* 1999. Principles and Performance of an Electron Spin Echo Spectrometer Using Far Infrared Lasers as Excitation Sources. *J. Magn. Reson.* **137**: 46-58.

Montgomery, C.G., Dicke, R.H. and Purcell, E.M. 1948. *Principles of Microwave Circuits*. New York, McGraw-Hill.

Müller, F., Hopkins, M.A., *et al.* 1989. A high magnetic field EPR spectrometer. *Rev. Sci. Instr.* **60**: 3681-3684.

Poole, C.P. 1983. *Electron spin resonance: a comprehensive trateise on experimental techniques*. New York, Wiley.

Poolton, R.J., Smith, G.M., *et al.* 2000. Luminescence sensitivity changes in natural quartz induced by high temperature annealing: a high frequency EPR and OSL study. *J. Phys. D: Appl. Phys.* **33**: 1007-1017.

Portis, A.M. and Teaney, D. 1958. Microwave Faraday Rotation: Design and Analysis of a Bimodal Cavity. *J. Appl. Phys.* **29**: 1692-1698.

Press, W.H., Teukolsky, S.A., Vetterling, W.T. and Flannery, B.P. 1992. *Numerical Recipes in C: The Art of Scientific Computing*. New York, Cambridge University Press.

Prisner, T., Rohrer, M. and MacMillan, F. 2001. Pulsed EPR spectroscopy: biological applications. *Annual Review of Physical Chemistry* **52**: 279-313.

Reijerse, E.J., van Dam, P.J., *et al.* 1998. Concepts in high-frequency EPR. Applications to bio-inorganic systems. *Appl. Magn. Reson.* **14**: 153-167.

Rohrer, M., Brugmann, O., Kinzer, B. and Prisner, T.F. 2001. High-field/High-frequency EPR spectrometer operating in pulsed and continuous-wave mode at 180 GHz. *Appl. Magn. Reson.* **21**: 257-274.

Rohrer, M., Krzystek, J., Williams, V. and Brunel, L.C. 1999. Fabry-Perot resonator for high-field multi-frequency ESR at millimeter and submillimeter wavelengths. *Meas. Sci. Technol.* **10**: 275-284.

Schmalbein, D., Maresch, G.G., Kamlowski, A. and Hofer, P. 1999. The Bruker high-frequency-EPR system. *Applied Magnetic Resonance* **16**: 185-205.

Seck, M. and Wyder, P. 1998. A sensitive broadband high-frequency electron spin resonance/electron nuclear double resonance spectrometer operating at 5-7.5 mm wavelength. *Review of Scientific Instruments* **69**: 1817-1822.

Smith, G.M., Lesurf, J.C.G., Mitchell, R.H. and Riedi, P.C. 1995. A high-performance mm-wave electron spin resonance spectrometer. *IEEE MTT-S Digest*: 1677-1680.

Smith, G.M., Lesurf, J.C.G., Mitchell, R.H. and Riedi, P.C. 1998. Quasi-optical cw mm-wave electron spin resonance spectrometer. *Rev. Sci. Instrum.* **69**: 3924-3937.

Smith, G.M. and Riedi, P.C. 2000. Progress in high-field EPR. *Electron Paramagnetic Resonance* **17**: 164-204.

Teaney, D.T., Klein, M.P. and Portis, A.M. 1961. Microwave Superheterodyne Induction Spectrometer. *Rev. Sci. Inst.* **32**: 721-729.

Ulrich, R. 1967. Far-infrared properties of metallic mesh and its complementary structure. *Infrared Phys.* **7**: 37-55.

van Tol, J. 2002. Personal communication.

Wei, Y.Z., Sage, J.T., *et al.* 1994. Protein Hydration Investigations with High-Frequency Dielectric Spectroscopy. *J. Phys. Chem.* **98**: 6644-51.

Wei, Y.Z. and Sridhar, S. 1990. Dielectric spectroscopy up to 20 GHz of lithium chloride-water solutions. *J. Chem. Phys.* **92**: 923-8.

Weis, V., Bennati, M., *et al.* 1999. High-Field DNP and ENDOR with a Novel Multiple-Frequency Resonance Structure. *J. Magn. Reson.* **140**: 293-299.

Wilmshurst, T.H., Gambling, W.A. and Ingraham, D.J.E. 1962. Sensitivity of Resonant Cavity and Traveling-wave EPR spectrometers. *J. Electron. Control* **13**.

Wylde, R.J. 1991. Gaussian beam-mode analysis and phase-centers of corrugated feed horns. *IEEE Trans. Microwave Theory Tech.* **MTT-41**: 1691-9.